Alma Mater Studiorum - Universita' di Bologna

Dottorato di Ricerca in Geofisica

Ciclo XXIV

Settore concorsuale di afferenza: 04/A4/Geo10: Geofisica della terra solida

# Deep geometry of subduction below the Andean belt of Colombia as revealed by seismic tomography

Candidato

Danilo Seccia

Coordinatore del Dottorato

Michele Dragoni

Relatore

Claudio Chiarabba

Esame finale anno 2012

# Abstract

In this research project new 3D tomographic models of Colombia were calculated. I used the seismicity recorded by Red Sismica Nacional de Colombia (RSNC) during the period 2006-2009. In this time period, the improvement of the seismic network yields more stable hypocentral results with respect to older data set and allows to perform new 3D Vp and Vp/Vs models. The final dataset consists of 10813 P- and 8614 S-arrival times associated to 1405 earthquakes. Tests with synthetic data and resolution analysis indicate that the velocity model is well constrained in central, western and southwestern Colombia to a depth of 160 km; the resolution is poor in the northern Colombia and close to Venezuela boundary due to a lack of seismic stations and seismicity. The 3D Vp and Vp/Vs models and the relocated seismicity indicate the existence of E-SE subducting Nazca lithosphere beneath central and southern Colombia. The changes in Wadati-Benioff zone geometries, Vp & Vp/Vs pattern, volcanism and seismicity, from North to South, show that the downgoing plate is segmented by slab tears roughly E-W directed, suggesting the presence of three different sectors. The seismicity volume of the northernmost sector represents most of the RNSC catalog and concentrated mostly on 100-170 km depth interval, beneath the Eastern Cordillera. In this area a massive dehydration was inferred, resulting from a delay in the eclogitization of a thickened oceanic crust in a flat-subduction geometry. In this sector a cluster of intermediate-depth seismicity (Bucaramanga Nest) is present beneath the elbow of the Eastern Cordillera and is interpreted as the result of massive and very localized dehydration phenomenon caused by an anomalous portion of hyper-hydrous oceanic crust, like a volcanic ridge. The central and southern sectors, although different in Vp pattern show, conversely, a continuous, steep

and more homogeneous Wadati-Benioff zone with overlying volcanic areas. Here a "normal-thickened" oceanic crust is inferred, allowing for a gradual and continuous metamorphic reactions to take place with depth, enabling the fluid migration towards the mantle wedge.

# Contents

# List of Figures

# List of Tables

# Acknowledgments

First of all, I would like to thank my PhD advisor Claudio Chiarabba, for his support throughout my studies. I'm grateful to him for introducing me in the world of scientific research and for being very open-minded. I am greatly indebted to Pasquale De Gori for the precious and friendly assistance during this years of collaborations. Thanks to Fabio Speranza and Claudio Faccenna for the constructive discussions and for providing relevant suggestions to improving the contents of this thesis. Thanks to German Prieto for the fruitful scientific collaboration in Bogotà. A special thank goes to Viviana Dionicio, for her friendly hospitality and assistance during the months spent in Bogotà. Thanks to all the people at INGEOMINAS-RSNC who have been made possible this study.

*Un ringraziamento speciale va alla mia "compagnuccia di banco" Marina, che mi ha supportato e sopportato durante questi ultimi mesi di lavoro febbrile sulla tesi. Grazie a Peppe e Betta per le pause-sigaretta al muretto e le chiacchiere in libertà. Un ringraziamento anche a tutti i "pollajoli" e ai colleghi-amici dei piani alti, con i quali ho condiviso momenti di scienza ma soprattutto momenti di svago, in particolare a Pamela, Michele, Mauro, Mario, Paola e Francesca. Grazie anche a Luigi, per tutte le sigarette che gli ho scroccato. Grazie a Federica per esserci stata, in un modo o nell'altro, in questi anni. Infine grazie ai miei genitori, che ancora mi sopportano dentro casa e continuano a credere in me.*

*Dedicated to my brother Alessandro*

# Chapter 1

# Introduction and summary

The Andean belt of Colombia provides a striking opportunity to investigate the geodynamics of northwestern South America. The tectonics is complex, resulting from the interaction of three different lithospheric plates: Caribbean, Nazca and South America. The structural style, the pattern of volcanism and the distribution of earthquakes make the region an intriguing challenge in the comprehension of subduction dynamics.

The deformed belts are the expression of a complicated tectonic assembly underlain by interacting oceanic slabs at depth. Previous studies have suggested relations between flat slabs, volcanism, and surface deformation in the more southerly Andes [Jordan et al., 1983; Gutscher et al., 1999; Gailler et al., 2007]. However, the tectonics of Colombia is still unclear and represents an interesting test-case for studying flat slabs vs. normal subduction. Underneath Colombia, the eastward subducting Nazca plate is inferred to be segmented by some slab tears. A smaller, southeast flat dipping slab, associated with the Caribbean plate, may be subducting, even if this feature

is under debate. Between these structures an intermediate-depth seismicity cluster ("Bucaramanga nest") is present, and the driving force is still unclear. The leading hypothesis are a slab-slab interactions, and/or dehydration embrittlement, or local heterogeneity of the downgoing plate. The previous models are, in general, not well constrained, and the forces involved in the processes not completely clarified.

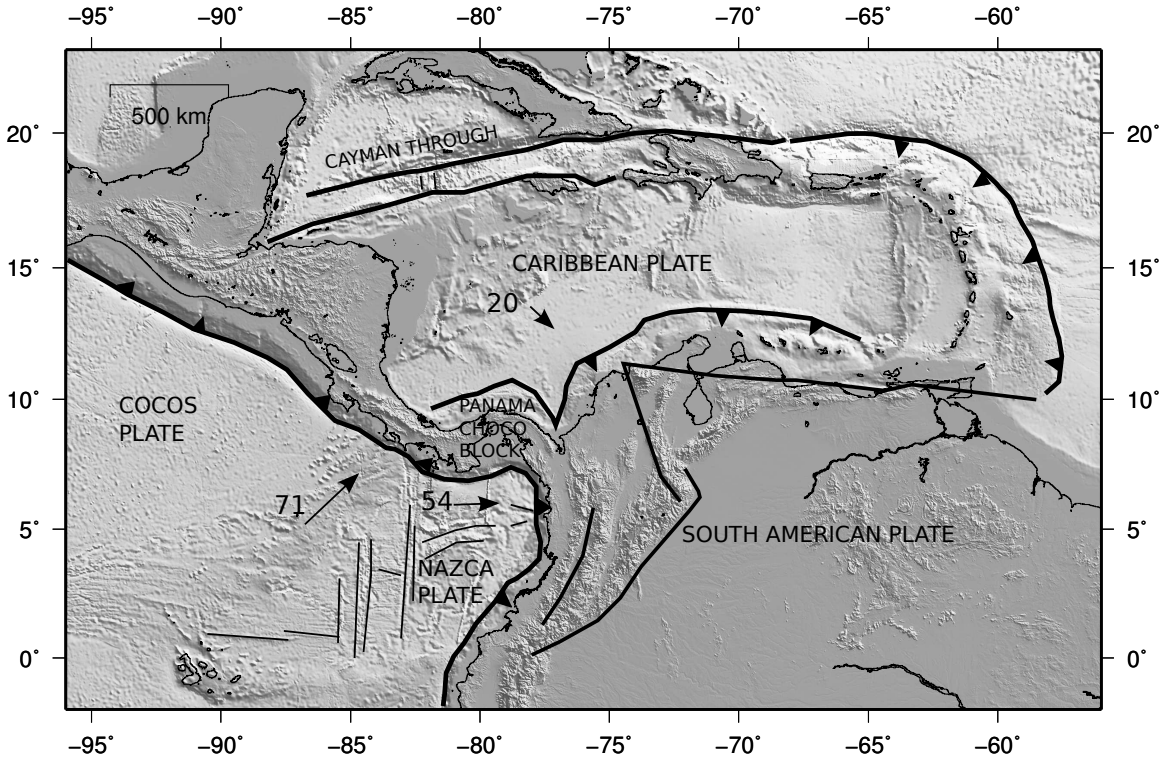


Figure 1.1: Regional scale tectonic context of Colombian Andes and northwestern South America with crustal velocity (mm/yr relative to stable South America)

The Colombian Andes represent a remarkable chance for a new seismological study because numerous intermediate-depth earthquakes can be used for imaging, and large along-strike variations in seismicity rate provide hints on deep dynamics and surface deformations. The region represents an ideal case-study to test subduction models (e.g. continuous slab dynamics vs. delamination), the origin of intermediate depth

seismicity, and the relations between magmatism and deep dynamics. The Colombian Andes developed from the collision of two major plates, Nazca and the Caribbean, and the Panama block. This leads to complex crustal motions and surface deformation [Taboada et al., 2000; Pennington, 1981; Trenkamp et al., 2002]. According to GPS data, with respect to the fixed South American plate, the Caribbean plate moves towards the east–southeast, while the Nazca plate motion is roughly towards the east, and the northern Andes motion is towards the northeast (Figure 1.1).

This complex pattern of plate motions produces a broad zone of continental deformation into the Colombian and Venezuelan Andes. The deformation is accompanied by a complex pattern of the shallow seismicity, occurring on many separate faults that are distributed over several hundreds of kilometers away from the accepted plate boundaries between the South American plate and the Nazca and Caribbean plates [Corredor, 2003]. There are remarkable tectonic features which need to be included in definitive dynamic models. For many topographic and structural elements only an ambiguous geodynamic explanations is provided. Large, along-arc variations in seismicity and volcanism exist (Figure 1.2), and abundant intermediate-depth seismicity delineates slab geometry and can be used for seismological imaging. This makes the region an excellent place to test continuous slab morphology change vs. tearing vs. break-off vs. lithospheric delamination modeling (e.g. close to tears or Bucaramanga).

The main objectives of this study are the improvement of the knowledge on the main seismogenetic structures underneath Colombia and the quality imaging of the subducting slab(s), to constrain depth, kinematics and spatial orientation of the sub-

duction system. The reconstruction of the slab geometries and interactions will help to understand the dynamics of Nazca subduction and will give new insights into plate tectonics in general. Colombia is a timely target for making major advances on these scientific issues because of the recent improvements in the political situation.

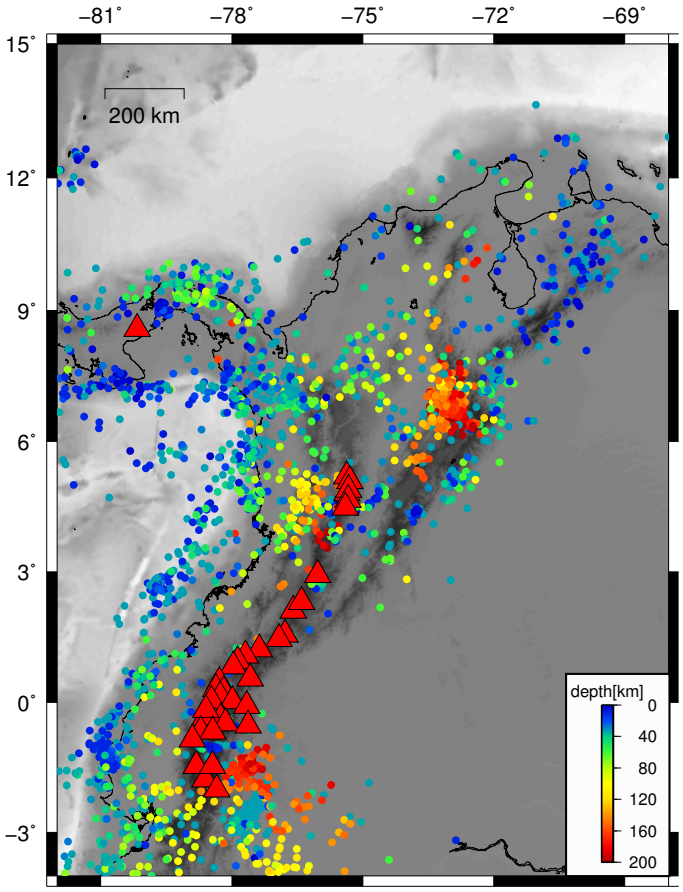


Figure 1.2: Seismicity and volcanism in northwestern South America. Earthquakes recorded in the time period 1993-2009 are shown. Ipocentral locations downloaded from National Earthquake Information Center website (NEIC - http://earthquake.usgs.gov/regional/neic/). Red triangles represent volcanoes.

This study has been made possible thanks to the cooperation between the *Istituto Nazionale di Geofisica e Vulcanologia* (INGV) and the *Instituto Nacional en Geologia y Minerìa* (INGEOMINAS), the Colombian institution which operates the National

Seismological Network of Colombia. The recent improvement of Colombian seismic network (from 2005) and the availability of new data from INGEOMINAS allow for the calculation of new velocity models enabling 3D quality imaging of subduction zones.

The thesis is organized as follows:

- Chapter 2 summarizes the relevant geological and geophysical background information from North West South America and Colombia. In order to understand seismogenesis and velocity information along the subduction zone it is necessary to define incoming and overriding plate characteristics through the subduction system.

- Chapter 3 provides the basic steps of the travel times inversion algorithms. The 3D seismic velocity structure, hypocenter locations and station corrections are calculated iteratively and simultaneously in a well constrained and worldwide adopted code, SIMULPS. The RKP ray-tracing was adopted in this study, being more robust in calculating long ray-paths with respect to the traditional ART-PB ray tracing, originally implemented in the code.

- Chapter 4 focuses on the Colombian Seismic Network and seismicity in Colombia. An outlook on recent development of the *Red Seismological Nacional de Colombia* (RSNC) is given. Special attention is paid on the presence of the Bucaramanga intermediate-depth seismic nest.

- Chapter 5 presents the results of the travel times inversion for 3D Vp and Vp/Vs

models, together with the resolution analysis and the synthetic tests.

- Chapter 6 provides interpretations on the the Vp and Vp/Vs tomographic models. The results indicate a strong heterogeneity of the subducting Nazca plate, partially segmented by some tears. The differential subduction process produces the tectonic assembly of Colombian Andes and the uneven distribution of deep seismicity. The Bucaramanga Nest could be related to a local anomaly of the downgoing Nazca plate, which produces massive and localized dehydration.

- Chapter 7 summarizes the main results obtained in this study. The new tomographic models give new insights into the structure of Colombian Andes, helping to understand the subduction dynamics.

# Chapter 2

# Tectonic setting

## 2.1 Andean belt of NW South America

The northern termination of the Andean chain along the northwestern margin of South America (SA) is a complex belt system, spreading northward like tree branches entering Panama and Venezuela [Pindell and Barrett, 1990; Taboada et al., 2000; Cortés et al., 2005]. The $\sim$ 200 km wide Andes of Ecuador expand northward to ca. 600 km, yielding the Western, Central, and Eastern Cordillera of Colombia. The Western Cordillera is in turn in tectonic contact with the Panama Arc, while at the northern margin of SA the triangular Maracaibo Block, bounded by strike-slip faults and narrow orogens, transfers deformation within Venezuela and Caribbean-SA boundary. To the south, these belts merge together and masking the original relationships and evolution. The northern termination of the Andean chain along the northwestern margin of South America (SA) is a complex belt system, spreading northward like tree branches entering Panama and Venezuela [Pindell and Barrett,

1990; Taboada et al., 2000; Cortés et al., 2005] (Figure 2.1).

The diffuse tectonic deformation of northwestern SA arises from its complicated interaction with the Nazca and Caribbean oceanic plates and the Panama Arc.

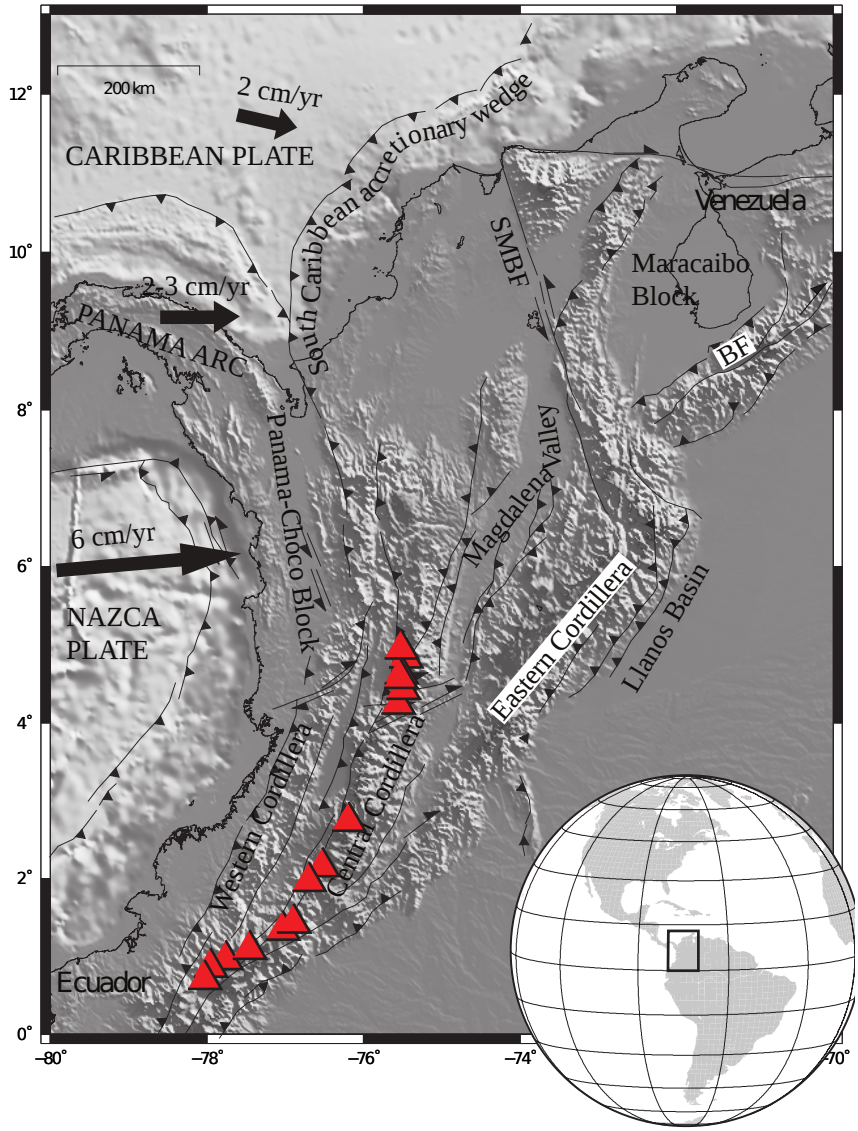


Figure 2.1: Shaded relief map of the North west South America. The major tectonic elements are shown. Black arrows indicate the crustal velocity relative to stable South America. Red triangles indicate volcanoes. The inset indicates the world location of the study area.

Global plate motion models [DeMets et al., 1990], along with GPS data gathered since the 1990s from SA, Panama Arc, and Pacific/Caribbean islands [Trenkamp et al., 2002] give a first-order picture of relative plate motion. The ca. 6 cm/yr E-W convergence between Nazca and SA is mainly (yet not completely) accommodated along the Nazca subduction zone, yielding $7.5 \leq M \leq 8.8$ earthquakes during the XX century. According to Trenkamp et al. [2002], a percentage of such convergence is transferred to the Andes of Colombia and the Maracaibo Block, which are escaping towards NE at 6 mm/yr. The Caribbean Plate is moving 2 cm/yr ESE with respect to SA, and its oblique convergence seems to be partitioned into a well-developed orogenic wedge (South Caribbean accretionary wedge), and a swarm of E-W right-lateral strike-slip faults. While the formation of the Western and Central Cordillera of Colombia has been routinely referred to the complex history of both Proto-Caribbean and Nazca subduction, and Cretaceous-Tertiary [Müller et al., 1999; Pindell and Barrett, 1990; Taboada et al., 2000; Cortés et al., 2005] accretion of oceanic and continental terranes to SA, the orogenic process generating the Eastern Cordillera has been a matter of long debate.

### The Eastern Cordillera of Colombia

The Eastern Cordillera is an intra-continental orogen inverting a late Jurassic-Cretaceous extensional basin [Colletta et al., 1990; Dengo and Covey, 1993; Mora et al., 2006]. It is a bivergent thick-skinned chain, with main eastward tectonic transport towards the Llanos foreland basin, and retro-vergent (westward directed) thrust sheets stacked in sequence towards the upper Magdalena Valley [Bayona et al., 2008;

Parra et al., 2009; Mora et al., 2010]. Although conglomeratic events, angular unconformities, and uplift inferred from thermochronological data have been referred to late Cretaceous-Tertiary tectonic episodes [Cortés et al., 2005; Parra et al., 2009], clear evidence for thrust-sheet emplacement onset in the Eastern Cordillera is constrained to mid Miocene times (ca. 15 Ma) during the "Andean" tectonic episode [Colletta et al., 1990; Dengo and Covey, 1993; Bayona et al., 2008]. Beneath the Eastern Cordillera, deep seismicity down to 160-170 km depth has been recorded [Taboada et al., 2000]. Seismicity is concentrated in the so-called "Bucaramanga nest" (Figure 2.1), continuously releasing small magnitude (M2.5-3.0, and no event with M larger than 6.0) earthquakes within a small mantle volume at 150-160 km depth [Zarifi et al., 2007]. Three different models have been proposed so far for the origin of the Eastern Cordillera. The first model relates the origin of the Eastern Cordillera to a low-angle SE-ward directed subduction of the Caribbean plate beneath NW SA [Taboada et al., 2000; Cortés et al., 2005]. The existence of a low-angle Caribbean slab beneath NW SA relies upon tomographic models by VanderHilst and Mann [1994], although a seismic Wadati-Benioff zone associated to the postulated slab has remained elusive so far. Another model suggest that deformation in the Eastern Cordillera is transferred from the to the Nazca subduction zone, via a "mid crustal detachment" branching from the Nazca subduction to the 500 km far Eastern Cordillera [Dengo and Covey, 1993; Cooper et al., 1995]. Colletta et al. [1990] suggested that the geometry of the Eastern Cordillera was due to the intracontinental subduction of the lithospheric mantle decoupled from overlying crust. The structural grain of the Cordillera oriental, shows the following remarkable features:

- The arcuate shape of the Cordillera results from the in situ inversion and reworking of early extensional fabric with very limited translation;

- Shortening decreases moving northward and southward from the elbow; the deformation of the Cordillera virtually ceased. Balanced cross section from 6°to 5°degree give an estimate of shortening around 100 km [Colletta et al., 1990; Sarmiento, 2001], 120 km [Taboada et al., 2000] or 140 km [Dengo and Covey, 1993] who adopted an eastward vergent, thin skinned model. Sarmiento [2001] also shows that the amount of shortening decreases southward. Balanced cross section on the Sabana de Bogota, from 4°to 5°N, gives from 58 km [Mora et al., 2009] to 70 km [Cortés et al., 2005]. To the south the eastern Cordillera deformation vanish jointing the western Cordillera. To the north it also slowly decreases in the Santander around at 8°-9°north.

- Considering the outward decreases of shortening, it is most probable that the growth of the eastern Cordillera initiate in the centre, where the deformation is maximum, and propagate northward and southward. The northern of the Cordillera is bounded by the Bucaramanga fault. It probably follow the same trend and decreasing its motion northward. Inside the Cordillera is dissected by strike slip faults running parallel to the Cordillera.

- There is limited evidence of volcanism in the Cordillera. Some small volcanic deposits have been refereed to Miocene. However, volcanism could be more diffuse than previously considered. Dolerite have been recently described near Bucaramanga [Jaramillo et al., 2005; Pardo et al., 2005] where a large geother-

mal field has been recently discovered.

# Chapter 3

# Method

Within the Earth, body wave propagation is a function of the velocity of the medium. In general there is a gradual variation of the seismic velocity with depth. However the Earth is not laterally homogeneous: crustal shortening, extensional processes and volcanoes produce structural heterogeneities and thus lateral velocity variations. Seismic tomography allows to image 3D velocity model of the subsurface to account for the lateral velocity variations.

## 3.1 Local Earthquake Tomography

Local Earthquake Tomography (LET) was introduced for the first time by Crosson [1976] and Aki et al. [1976]. Let is a powerful technique to investigate the subsurface and has been widely and successfully applied in various tectonic contexts.

The arrival time of a seismic wave at a station is a non-linear function of the hypocentral parameters and velocity field [Kissling et al., 1994]. LET allows to resolve

the initial estimates of the model parameters (velocity and hypocenter) by perturbing them in order to minimize the misfit between predicted and observed arrival times. In general, solutions are obtained by linearization with respect to a reference 1D Earth model and starting hypocentral coordinates, and the resulting tomographic images are thus dependent on the initial reference model and starting hypocentral locations. The only knowns in the LET problem are the receiver locations and observed arrival times. The source coordinates, origin times, and velocity field are unknown parameters. Therefore, the input data for every tomographic algorithm consist of the absolute arrival times from local seismic events and station coordinates.

According to ray theory, travel time $T$ from the source $i$ to the receiver $j$ is expressed as:

$$T_{ij} = \int_{source}^{receiver} uds \tag{3.1}$$

where $u$ is the slowness $(1/V)$ along the ray path. As described above the input data for LET are the arrival times, defined as:

$$t_{ij} = t_0 + T_{ij} \tag{3.2}$$

where $t_0$ is the origin time of the event. Given a set of arrival times $t^{ij}$ recorded by a seismic network, synthetic arrival times are calculated by equations 3.1 and 3.2 by iteratively perturbing hypocentral and velocity parameters in order to minimize the residuals between observed and predicted arrival times:

$$r_{ij} = t_{ij}^{obs} - t_{ij}^{calc} \tag{3.3}$$

Since direct solutions of the problem are in general not possible, it can be linearized and solved iteratively, if an initial guess of the model parameters close to the true solution is available. The concept of minimum 1-D model was introduced by [Kissling, 1988] referring to the 1-D model with corresponding station corrections that lead to the smallest possible uniform location error for a large set of well-locatable events. The main purpose of a minimum 1-D model is to provide an adequate reference model for 3-D tomography, ensuring that the linearization represents a solution as close as possible close to the true model [Kissling et al., 1994]. The problem may be further complicate by several factors: (1) seismic ray paths generally are not straight and are a function of the velocity model itself, (2) the distribution of seismic sources and receivers is sparse and non-uniform, (3) the locations of the seismic sources are not well known and often trade off with the velocity model, and (4) picking and timing errors in the data are common [Shearer, 1999].

The tomographic code used in this study, SIMULPS, was developed by Thurber [1983], who introduced an iterative simultaneous inversion for 3D velocity structure and hypocenter parameters using parameters separation and an approximate ray tracer. The code has been further developed through the years [Eberhart-Phillips, 1990; Haslinger, 1998] and is one of the most widely applied. Earth structure is parameterized assigning velocity values of the reference 1-D velocity model to a 3-D grid of nodes. Velocity in a certain point of the model is provided by a linear interpolation between model nodes. The inversion process is terminated when a number of specified iterations is reached, or when the variance reduction ceased to be significant, according to a f-test. The adjustments of the model are obtained by minimizing the arrival

time residuals with a damped least square algorithm. For an array of earthquakes and receivers, the arrival time residuals equation can be written in matrix notation as:

$$\mathbf{d} = G\,\mathbf{m} \tag{3.4}$$

where the vector **d** contains the arrival time residuals for all observations, the matrix G the partial derivatives for hypocentral and velocity parameters, and the vector **m** the model perturbations in hypocenters and velocity. To solve the equation for **m**, the inverse of the matrix $G$ is computed. Usually there is no unique solution to the problem becouse there are numerous undersampled nodes and/or tradeoffs in the perturbations between different nodes Shearer [1999]. This is generally due to a non-uniform distribution of sources and receivers which produces irregular ray distribution, rendering overdetermined and underdetermined model parameters in the same problem. A damping parameter ($\theta$) is thus introduced to avoid very small or zero eigenvalues for the underdetermined parameters, which can introduce instabilities in the solution. In a damped least square sense, the equation 3.4 is resolved by:

$$\mathbf{m} = (G^T G + \theta^2 I)^{-1} G^t \mathbf{d} \tag{3.5}$$

In order to facilitate computation of the inversion, **m** is split into a part containing only the velocity parameters and one containing only hypocentral parameters, but retaining the formal coupling between both [Pavlis and Booker, 1980]. Thus, using parameter separation, the earthquakes are relocated separately with the updated velocity model after the inversion for model parameters. The modelling is thus an iterative process due to the linearization and the damping. Damping depends mainly on

model parametrization and on the average observational error (a priori data variance) [Kissling et al., 2001] and can be determined by analyzing trade-off curves between model variance and data variance for single-iteration inversions [Eberhart-Phillips, 1986]. Appropriate damping values show a significant decrease in data variance without a strong increase in model variance, leading to the simplest model to fit the data. SIMULPS is able to solve for Vp and Vp/Vs using P and S-P travel times, respectively. In most earthquake datasets the quantity and quality of S-wave arrival times are significantly decreased with respect to the P-wave data, this causes great variations in possible artifacts and modelling errors which are minimized by inverting for Vp/Vs instead of Vs [Evans et al., 1994].

### 3.1.1 Resolution

To test the reliability of the tomographic models, the analysis of the Resolution Matrix (RM) is computed. Model resolution depends on data quality, node spacing and ray coverage in the volume considered. RM [Menke, 1989] is a square matrix $M$, where $M$ represent the total number of the inverted parameters:

$$R = (M^T M + \theta^2) M^T M \tag{3.6}$$

Each row of RM contains information on the volumetric estimate of parameters. A perfectly resolved node is characterized by a compact averaging vector with elements close to 1 on the diagonal and 0 elsewhere. The sharpness of the averaging vector is quantified by means of the Spread Function (SF) as defined by Michelini and McEvilly [Michelini and McEvilly, 1991]:

$$S_j = \log \left[ |s_j|^{-1} \sum_{k=1}^{N} \left( \frac{s_{kj}}{|r_j|} \right)^2 D_{jk} \right] \tag{3.7}$$

where $s_{kj}$ are the elements of the resolution matrix, $R$, and $D_{jk}$ are the distances in kilometers between pairs of nodes. Each row of the resolution matrix contains P- and S-velocity parameters. In equation 3.7, the elements of the resolution matrix are normalized such that the sum of their squares is equal to one. $|s_j|$ is the $L_2$ norm and can be interpreted as a weighting factor that takes into account the value of the resolution kernel for each parameter. The SF compresses each row of the resolution matrix into a single number that describes how strong and peaked the resolution is for that node [Toomey and Foulger, 1989]. The smaller the SF value, the better the resolution for the model parameter. The variation of SF is controlled by node spacing and damping. The higher the distance between two nodes the higher is the value of SF. High damping values produce high values of SF. Usually a well constrained model parameter has a SF value lower than the grid node spacing.

Thurber defines a useful measure of the sampling of nodal locations, the derivative weight sum (DWS) [Thurber and Eberhart-Phillips, 1999]. The DWS provides an average relative measure of the density of seismic rays near a given velocity node. This measure of seismic ray distribution is superior to an unweighted count of the total number of rays influenced by a model parameter, since it is sensitive to the spatial separation of a ray from the nodal location. The DWS of the $n-th$ velocity parameter $\alpha_n$ is defined as:

$$DWS(\alpha_n) = N \sum_i \sum_j \left\{ \int_{P_{ij}} \omega_n(x)\, ds \right\} \tag{3.8}$$

where $i$ and $j$ are the event and station indices, $\omega$ is the weight used in the linear interpolation and depends on coordinate position, $P_{ij}$ is the ray path between $i$ and $j$, and N is a normalization factor that takes into account the volume influenced by $\alpha_n$. The magnitude of the DWS depends on the step size of the incremental arc length $ds$ used in the numerical evaluation of equation 3.8. Smaller step length yield larger DWS values; therefore, DWS provides only a relative measure of ray distribution and its unit of distance are unimportant. Poorly sampled nodes are marked by relatively small values of DWS. In practice, it is useful to monitor changes in the spatial variation of the DWS while testing for an optimum nodal configuration [Thurber and Eberhart-Phillips, 1999]. A good parametrization, in general, maximizes the number of parametric nodes within a volume and, for a damped least squares inversion, minimizes the number of poorly sampled nodes.

### 3.1.2 Ray-tracing

The resolving power of ray tomography depends on the accuracy of the forward calculations, i.e. the determination of the propagation path and travel time through the velocity model [Haslinger and Kissling, 2001]. The code used in this study, SIMULPS 14, includes two ray tracing methods. The original is the pseudo bending ray tracer (ART-PB) [Um and Thurber, 1987], in which the initial travel times are computed for a set of arcs with different radii and laying in different planes, connecting the source and the receiver; the arc that corresponds to the smallest travel time is then chosen and perturbed by pseudo-bending, i.e. the segment endpoints are moved in the direction of the largest velocity gradient. The second ray tracer (RKP) is a full

3-D shooting and perturbation algorithm, in which they ray connecting station and source is determined by varying initial azimuth and take-off angles at the source; the variation of the initial angles is performed by using first-order perturbation theory [Virieux et al., 1991; Haslinger, 1998]. Initial shooting angles for the RKP ray tracing are obtained by ART-PB ray tracing on the first iteration; subsequent ray tracing iterations use the previously determined shooting angles as initial values [Haslinger and Kissling, 2001]. Usually, the endpoint of a ray calculated by shooting methods does not coincide with the station location; the accuracy to which the ray path coincides with the receiver is specified by the user, considering, for example, the station location uncertainty. Using synthetic model testing, [Haslinger and Kissling, 2001] determined that both ray tracing schemes are precise within $\pm 10$ ms in travel time for ray lengths inferior to 60 km, but for longer rays, the RKP technique yields significantly smaller errors, outperforming the ART-PB.

Becouse of the large areas considered, the poor and non-uniform station coverage and the uneven distribution of earthquakes both in horizontal direction and in depth, the RKP ray tracing was preferred to the traditional ART-PB in the Colombian case study, allowing for the calculation of longer ray paths.

# Chapter 4

# Seismic network and seismicity

## 4.1 Red Sismica Nacional de Colombia (RSNC)

Seismic data used in this study are those recorded by the *Red Sismica Nacional de Colombia* (RSNC), the National Seismological Network of Colombia. The availability of data from RSNC was made possible thanks to the cooperation between INGV and INGEOMINAS, the Colombian institution which operates the seismic network.

Pulido [2003] gives a complete revision of the history and recent development of RSNC as summarized in the following. The National Seismological Network of Colombia (RSNC) was sponsored by several Colombian agencies (National Office for Prevention and Attention of Emergencies and the Colombian Telecommunications Agency) as well as the Canadian Development Agency . The RSNC started its operation in June 1993 and consists of 20 seismic stations countrywide connected to a central station by a satellite system. The seismometers are Teledyne Geotech S-13 vertical component with a period of 1s. The data is digitized at 16 bits and 60 sps

with a dynamic range of 136db [Nieto and Escallon, 1996]. The detection threshold of the network is M4.0 in the northern part of Colombia where the stations are sparse, M3.5 in the western part (78°W to 80°W), and M2.0 in the central part. From June 1993 to June 1999, the RSNC has recorded 15581 earthquakes, mostly located in the central part of the country [Ojeda and Havskov, 2001]. Monthly bulletins describing the seismic activity countrywide are published. Simultaneously to the RSNC, in 1993 INGEOMINAS started the deployment of the National Strong Motion Network of Colombia (RNAC), which was entirely sponsored by the Colombian government. The RNAC consists of 120 strong motion digital accelerographs countrywide, including a local network at Bogotà city consisting of 29 instruments. The instruments are KINEMETRICS ranging from 12 to 19 bits of resolution (RSNC and RNAC homepage, INGEOMINAS). The local network at Bogota has been operating since 1999 and was installed following the recommendations of a Seismic Microzonation Project of Bogota [INGEOMINAS, 1997]. The Bogota network also includes three borehole instruments located at 115 m, 126 m and 184 m of depth [Ojeda et al., 2002]. The RNAC annually publishes a Strong Motion Bulletin as well as a special issues for large earthquakes. INGEOMINAS also operates three volcanic observatories that monitor the activity of the two volcanic regions in Colombia. Besides to the RSNC and RNAC, since 1987 a seismological network in the South-West of Colombia (OSSO) is operated by Universidad del Valle, as well as a local strong motion network at Medellin city, the second largest city of Colombia, operated by EAFIT. In the period 2005-2006 a process of updating and expanding of the Seismological and Volcanological System of Colombia is started, projected to the years 2011-2012. The aim is to expand networks

and broadband technology purchase. At present RSNC has 34 permanent stations installed, 13 broadband and 21 short period (Figure 4.1). It also has regional stations in subnets and volcanological observatories.

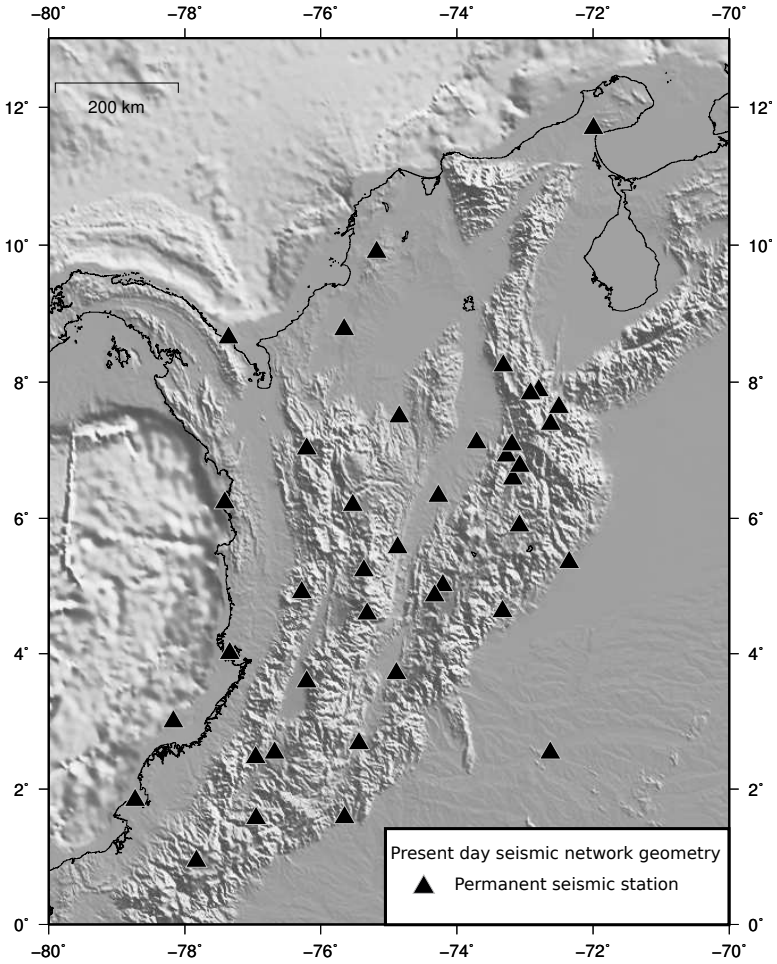


Figure 4.1: Colombian seismic network in its present-day configuration.

Earthquake locations are routinely performed at INGEOMINAS. Phase picking and locations were accomplished using the SEISAN software package [Havskov and Ottemoller, 2005], which includes the program HYPO71 [Lee et al., 1975]. The soft-

ware was chosen because it provides a complete set of programs and a simple database structure for analyzing earthquakes, allowing phase picking with a cursor, event location, determination of spectral parameters, seismic moment, focal mechanisms, etc. A weighting scheme for quality of the P- and S-arrivals was applied. It is based on the picking uncertainty caused by noise. The weights were assigned following the HYPO71 definition. In the Figure 4.2 the seismicity recorded by RSNC during the period 1993-2009 is shown.

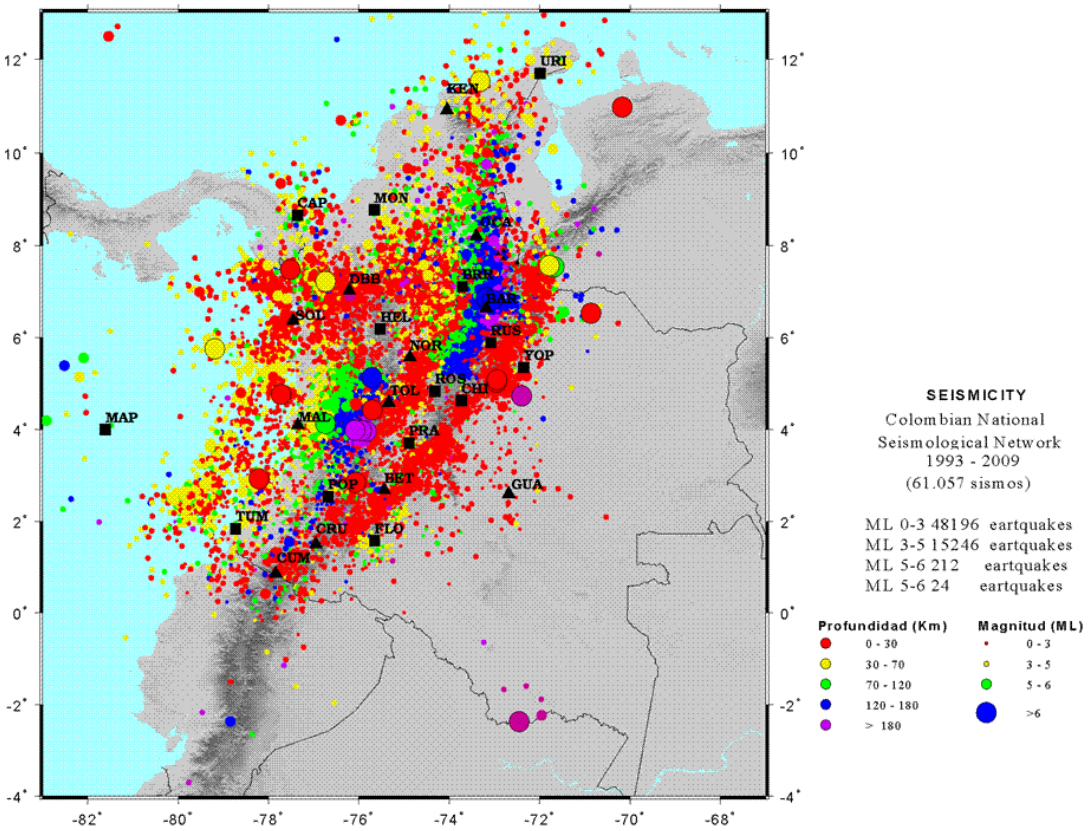


Figure 4.2: Seismicity recorded by RSNC during the period 1993-2009.

## 4.2 Seismicity of Colombia

In this study I used the entire seismic data recorded by RSNC during the years 2006-2009. In this time period, the improvement of the seismic network yields more stable hypocentral results with respect to older data set and allows to perform new 1D and 3D Vp and Vp/Vs models. A total of 20135 earthquakes were relocated using the HYPOELLIPSE code [Lahr, 1999] with the 1D model of Ojeda and Havskov [2001]. The Moho depth is fixed at 32 km depth and confirmed by the analysis of travel-time vs. distance curve (not shown here). The Vp/Vs ratio was calculated by means of the Wadati diagram (Figure 4.3). The obtained value of 1.78 is in agreement with the value calculated by Ojeda and Havskov [2001].

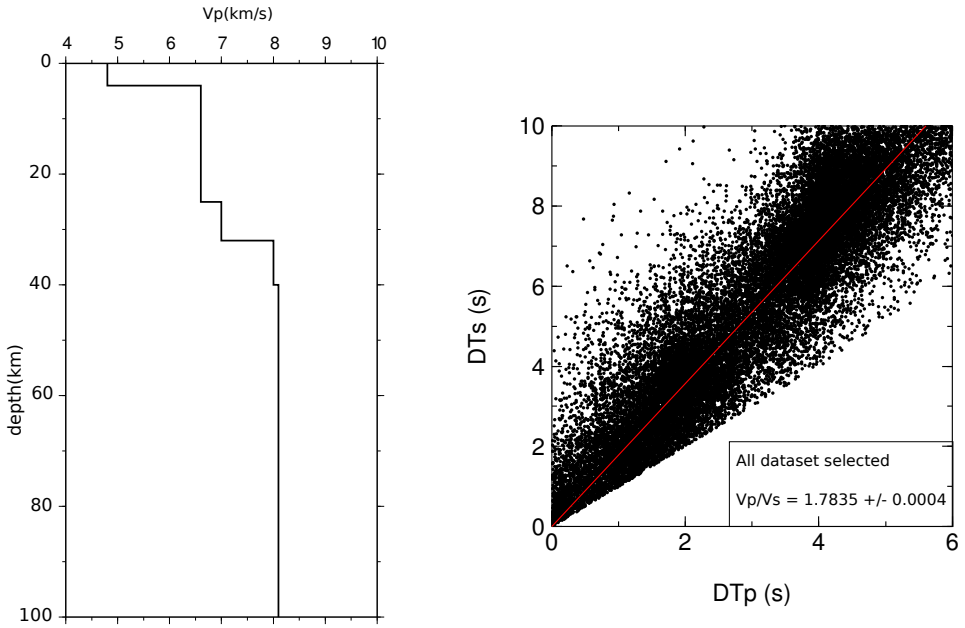


Figure 4.3: 1D Vp model of Ojeda and Havskov [2001] used for earthquake location (left); Wadati diagram for all the analyzed events reporting the differences between P and S arrivals for each couple of station. The double differences are fitted by a linear regression. The slope of the red solid line is the Vp/Vs ratio (right).

Despite the non-uniform station coverage and the extension of the study area, the earthquakes are fairly well located in 1D preliminary location.

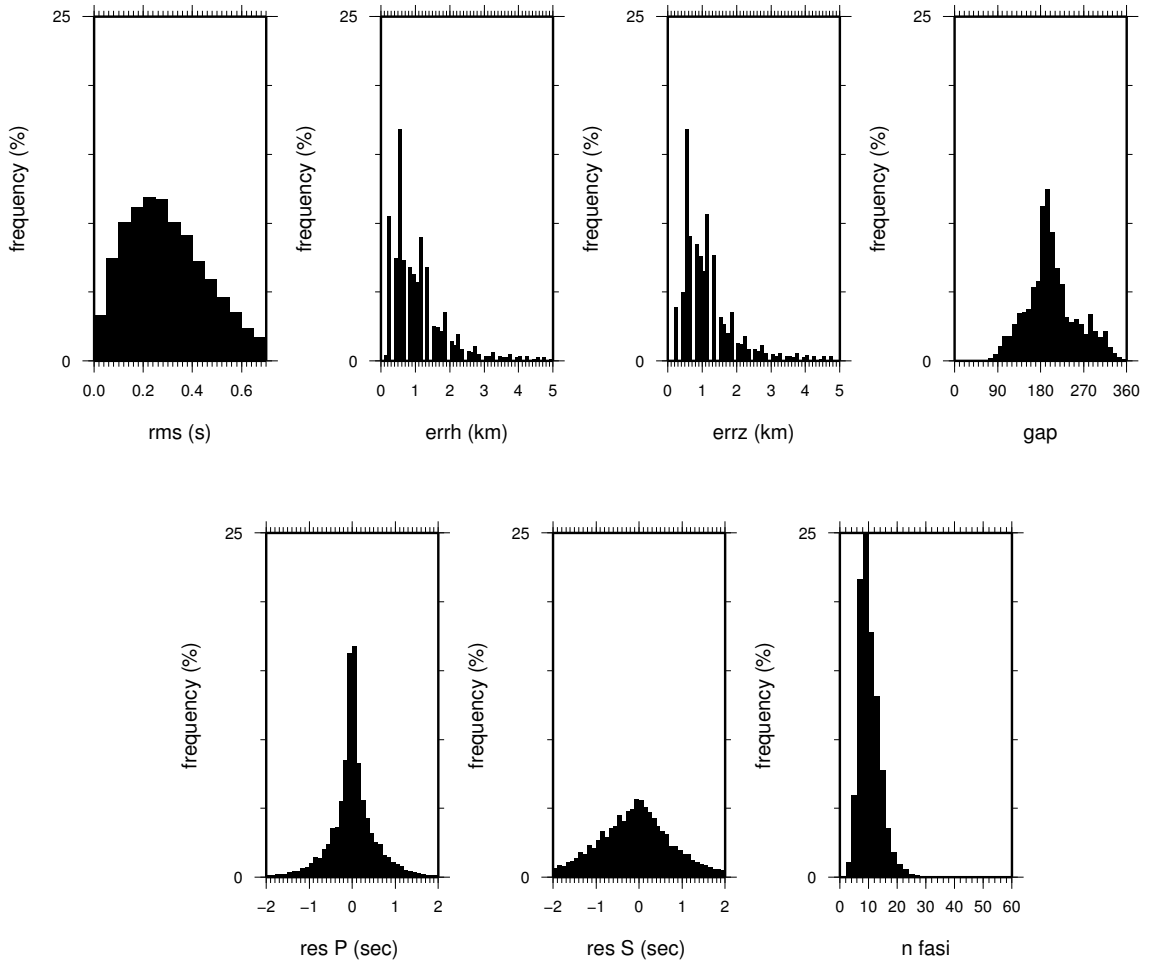


Figure 4.4: Final location rms, horizontal and vertical errors, azimuthal gap for the locations of the whole data set, histograms of P-wave and S-wave residuals and events frequency with phases number of the whole data set.

In general, the vertical and horizontal error (Figure 4.4) are less than 5 km and the P-phase residuals are strongly peaked on the zero. The S-residuals histogram is smooth and plausibly many S phases are affected by large reading errors. This

occurrs becouse, the S phases were often picked on the vertical component of the waveform. Furthermore, the recorded signal results complicated by the long distance travelled from the source to the receiver, since the majority of the earthquakes occurr at 120-160 km depth. Most of the seismicity occurrs in the Bucaramanga Nest area. The remaining is located at the borders of mountain ranges and in the nearby of the Pacific coast.

In figure 4.5 a selection of well constrained earthquakes is shown. Hypocentral locations of events with at least 10 arrivals (P+S phases), a rms value less than 0.5 s. and a maximum azimuthal gap of 200° are plotted in map and in cross-sections. A total of 3457 earthquakes is shown.

*Shallow seismicity.* The seismicity defines most of the active zones of the crust along the borders of mountain ranges. The shallow seismicity across the country is associated with the N-NE trending faults within the cordilleras. To the east the seismicity clearly delineates the Eastern Cordillera Frontal Fault along its entire length from Ecuador to Venezuela.

*Deep seismicity.* The selected hypocenters reveal two distinct E-SE dipping Wadati-Benioff planes beneath Colombia (Figure 4.5). Hypocenters south of 5°N clearly depict the Nazca Wadati-Benioff zone, deepening SE-ward beneath the Western and Central Cordillera. Several active volcanoes are located at 150-200 km above the Wadati-Benioff zone. Between 5°and 7°N, deep seismicity along the Nazca subduction zone almost disappears (and no volcanism occurs), while a subparallel but distinct (it is shifted inland by ca. 200 km) Wadati-Benioff plane (dipping 45°towards SE and reaching 200 km depth) appears beneath the Eastern Cordillera.

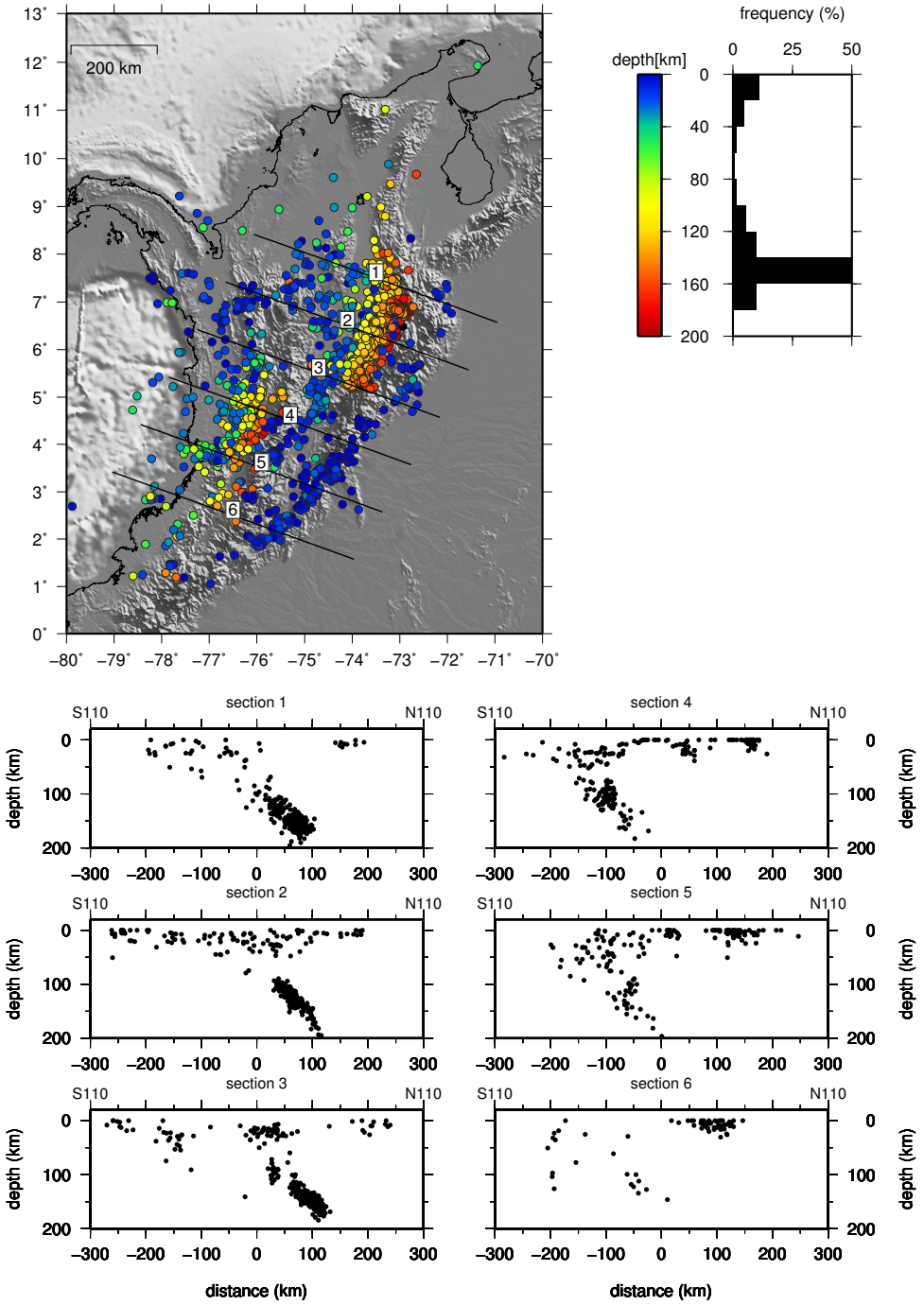


Figure 4.5: Epicentral locations and depths of 3457 selected earthquakes. Hypocentral locations of 3457 events are shown. The six cross-sections in the lower portion of the plot show the projection (in a band wide of 50 km) of the hypocenters (see locations in the map). In the upper right corner of the figure a depth-frequency seismicity histogram is also reported.

The distribution of the seismicity along the strike of the Cordillera shows an abrupt shut of deep seismicity south of 5°N, a volume of seismicity descending down to 180-200 km depth from 5°to 8°N, and then a progressive shallowing of the earthquake hypocenter up to 9°N. The intense nest is located right in the centre of the Cordillera elbow. Comparison between deep seismicity and topography show that the deeper portion of the seismicity corresponds to the higher topographic relief (Figure 4.5, map). To the north the progressive shallowing of the seismicity well agree with the one of the topography. To the south, the shallowing in topography is 100 km to the south of the shut off in the seismicity, probably indicating that interaction with the Nazca slab is more evident. In this area the good fit between seismicity depth and topography indicates that regional crustal thickening, where elevation is higher, corresponds with region of deeper earthquake. Hence, earthquake distribution could be interpreted as a result of the internal dynamic of the Eastern Cordillera evolution.

### 4.2.1 Bucaramanga Nest

The areas of persistent and clustered seismicity are in general defined as seismic nests. In a few places in the world such seismicity occurs at indermediate-depth (70-280 km depth). The main characteristics of a seismic nest are the high activity relative to the surroundings, the concentration of hypocenters in a small volume and the continuity of seismic energy release. Within this definition, two types of nests can be distinguished: shallow nests usually related to volcanic activity and intermediate-depth nests related to subduction zones processes [Zarifi, 2007]. The shallow nests are well documented in many region of the world. For example, some nests in Japan

(Kanto district) have been suggested as shallow nests, with high rate of energy release [Usami and Watanabe, 1980]. Similar activity has been seen near volcanic areas in Central America [Stoiber and Carr, 1973], in New Zealand [Blot, 1981a], in New Hebrides [Blot, 1981b] and in the Aleutians [Engdahl and Scholz, 1977]. More than 40 such nests are identified in the circum Pacific and Indonesian arcs. This type of seismic nests can then develop by stress concentration at the margins of the weak zones of the volcanic areas [Carr, 1983].

Zarifi [2007] made a detailed and complete analysis on the known intermediate-depth seismic nests in the world. Only three intermediate-depth nests are documented in literature: the Bucaramanga nest in Colombia (hereinafter BN) at 6.8°N and 73.1°W, centered at 160 km depth [Tryggvason and Lawson Jr, 1970; Ojeda and Havskov, 2001; Frohlich et al., 1995; Schneider et al., 1987, 1972]; Vrancea in Romania at 45.7°N and 26.5°E at depths between 70 and 180 km [Gusev et al., 2002]; the Hindu Kush in Afghanistan [Pegler and Das, 1998]. In deepest nest, Hindu Kush, the earthquakes tend to occur as clusters of events but the most are located at 36.5°N and 71°E in depth between 170-280 km. The focal mechanisms of earthquakes in Hindu Kush and Vrancea show reverse faulting, while in Bucaramanga the focal mechanisms are variable but the majority have reverse mechanisms (fig 4.6). Many studies agree that the seismicity in Vrancea is the result of progress of slab detachment from its upper part (slab break-off) or delamination [Koulakov et al., 2010]. The driving force in Hindu kush is yet unclear, the hypothesis are a distorted slab or a collision of two subducting slab from opposite directions.

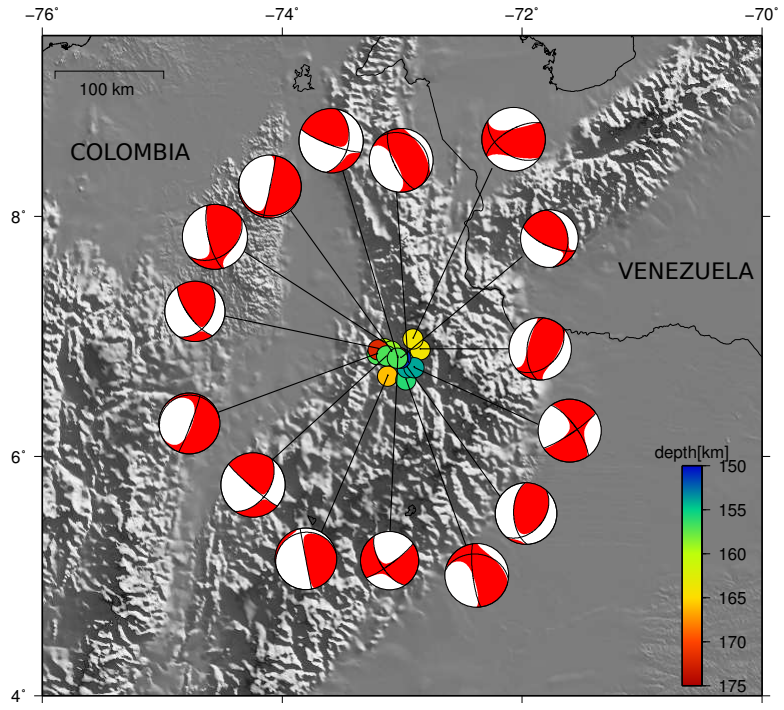


Figure 4.6: The Harvard CMT solutions (data from 1976 to 2009) for the earthquakes in 150-175 km depth interval. in BN area.

The smallest nest is the BN (fig 4.7), representing $\sim 50 - 75\%$ of the entire RSNC's catalog. With respect to Vrancea and Hindu kush, the BN has the highest activity rate per unit volume [Zarifi and Havskov, 2003]. There are many studies about this nest with both local and teleseismic data, which all show that the BN has a small volume. For instance Tryggvason and Lawson Jr [1970] and Schneider et al. [1972] claimed that the BN is less than 10 km in radius. Schneider et al. [1987] found that the nest has a volume of about 8 km (NW) by 4 km (NE) by 4 km (depth) centered at 161 km depth. Pennington et al. [1979] suggested that the nest has a source volume with a diameter of 4-5 km. All of these values are based on local data. Using teleseismic data, Frohlich et al. [1995] found a volume of about $11 \times 21 \times 13$ $km^3$.

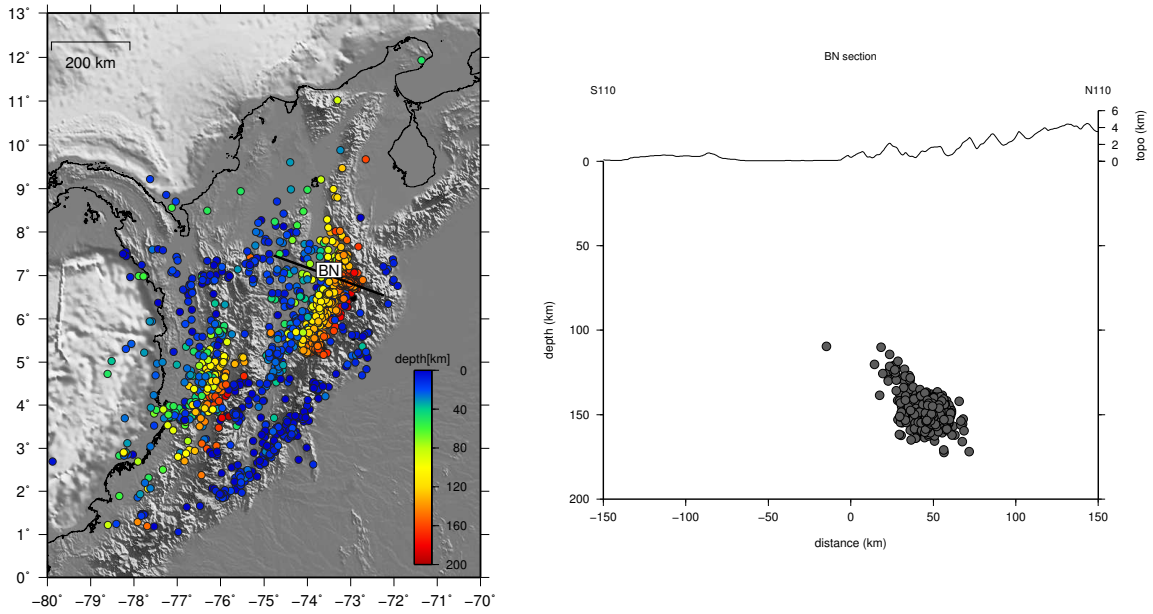


Figure 4.7: A close look to the BN. The cross-section location is shown in the map (left).

In the BN About no events larger than M6.0 are observed, the reason is still unknown. The mechanism producing BN "anomaly" is still unclear and under debate. Earthquakes deeper than 60 km represent 25% of global seismicity. With increasing depth, pressure and temperature should in theory prevent brittle failure. Many studies suggest that in BN, the driving mechanism is fluid migration or dehydration processes resulting from metamorphic reactions [Jung et al., 2004; Hacker et al., 2003b; Preston et al., 2003]. An alternative hypothesis is a complex concentrated stress field resulting from slabs interaction.

# Chapter 5

# Velocity structure

In this chapter, the tomographic inversion is described. From the relocated database, the earthquakes with the best quality, (i.e. well constrained), are selected to perform a Local Earthquake Tomography. The preferred solution is then examined through resolution assessment tools and synthetic tests. Furthermore, a detailed description of the resolved velocity structure is provided. Most of the contents of this chapter are in preparation for publication.

## 5.1 LET

For the tomographic inversion the dataset was edited on the basis of a preliminary hypocenter location with the initial reference 1D-velocity model: I selected a subset of earthquakes with at least 6 P- and 4 S-readings, azimuthal gap less than 180°and location uncertainty less than 5 km. Applying these criteria, 1405 events recorded by 65 seismic stations were selected for the inversion resulting in 10813 P-wave and

8614 S-wave travel time observations. Assessing the appropriate model parametrization is complicated by the fact that resolution estimates are strongly affected by the chosen model parametrization [Kissling et al., 2001]. Coarse grid spacing yields large resolution estimates, whereas fine-grid spacing yields low resolution estimates.

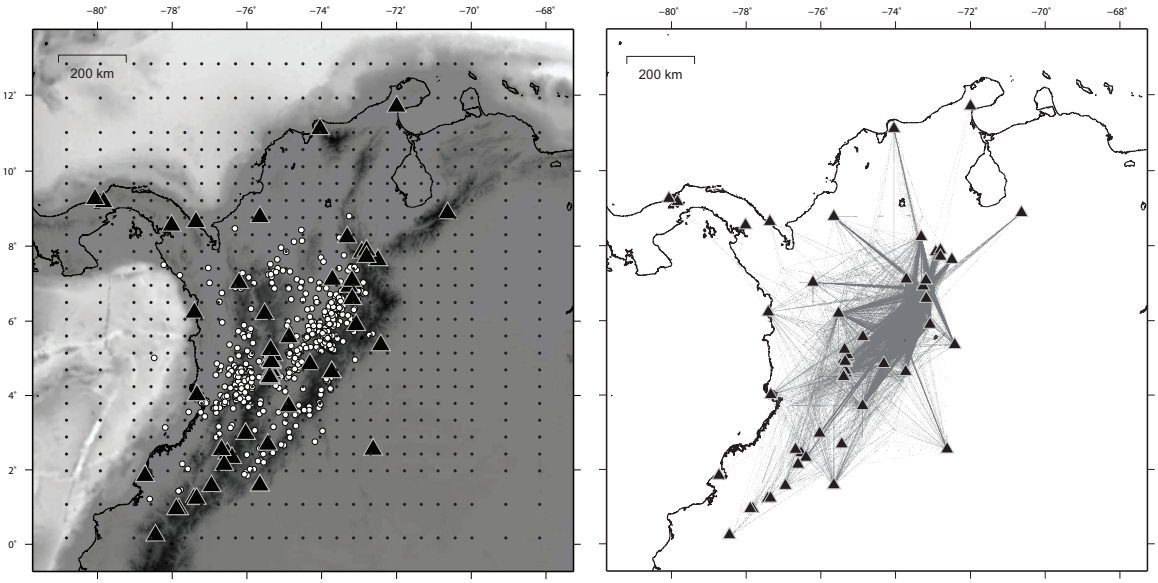


Figure 5.1: Left: Hypocentre locations (white circles), stations (black triangles), and grid nodes (gray dots) used in the inversion (left). Right: ray-coverage of the P-data set. Black triangles denote stations.

The station and earthquake distribution is highly non-uniform in Colombia (Figure 5.1). There are many areas with poor station coverage and low seismicity rate, demanding a large grid node spacing. Different grid spacing were investigate and finally 50 km horizontal grid spacing was choosen. Vertical grid node spacing varies between 10 km at shallow depth ($< 60$ km) and 20 km at greater depth ($> 60$ km). Velocities of the reference 1-D model from Ojeda and Havskov [2001] (Figure 4.3) were interpolated at depth to match the gradient formulation used in SIMULPS14. This model parametrization represents the finest possible model grid spacing without

showing a strongly heterogeneous pattern of the DWS. The derivation of a minimum 1D-model Kissling [1988](not shown here) yielded no significant differences with respect to 1D-model of Ojeda and Havskov [2001], in terms of layering, absolute velocity value, and rms reduction. Consequently, the 1D model of Ojeda and Havskov [2001] was choosen as reference 1D model.

Damping is a critical parameter in the inversion [Kissling et al., 2001] because it affects both results and resolution estimates such as the diagonal element of the resolution matrix. High damping values yields low model perturbations and low resolution, whereas low damping yield high model perturbations and good resolution. Damping depends mainly on model parametrization and on the average observational error (a priori data variance) [Kissling et al., 2001] and can be determined by analysing trade-off curves between model variance and data variance for single-iteration inversions [Eberhart-Phillips, 1986].

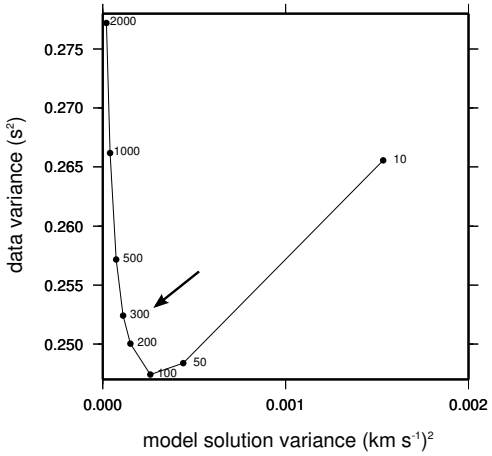


Figure 5.2: Trade-off curves to determine damping parameter. The selected value is indicate by the black arrow.

Appropriate damping values show a significant decrease the in data variance without a strong increase in the the model variance, leading to the simplest model to fit the data. Figure 5.2 displays the trade-off curve for the tomography data set. I finally selected a damping value of 300 (see Figure 5.2) that decreased data variance significantly without strongly increasing the model variance, thus yielding a smooth solution. A damping value of 200 would also be well suited, but I preferred to select a higher and conservative damping value to avoid instabilities during the inversion.

The inversion was iterated until the variance improvement ceased to be significant, according to a f-test. The variance was reduced of 39% after 4 iterations (see Table 5.1).

| Inversion parameters | |
|---|---|
| Earthquakes | 1405 |
| P observations | 10813 |
| S observations | 8614 |
| No. of stations | 65 |
| Iteration steps | 4 |
| Damping | 300 |
| Variance Reduction | 39% |

Table 5.1: Tomographic inversion - summary

## 5.2 Solution quality

To test the reliability of the tomographic models, a complete analysis of the Resolution Matrix (RM) for Vp and Vp/Vs models has been performed. Each row of RM contains information on the volumetric estimate of parameters. A perfectly resolved node is characterized by a compact averaging vector with elements close to 1 on the diagonal and 0 elsewhere. The sharpness of the averaging vector is quantified by

means of the Spread Function (SF) as defined by Michelini and McEvilly [1991]. The SF compresses each row of the resolution matrix into a single number that describes how strong and peaked the resolution is for that node [Toomey and Foulger, 1989]. The smaller the SF value, the better the resolution for the model parameter. From the analysis of DWS vs spread function [Toomey and Foulger, 1989] (Figure 5.3) I choosed 3 as cutoff value of SF for both Vp and Vp/Vs models. The solution quality is further verified by sensitivity and resolution tests using checkerboard and synthetic models for Vp.

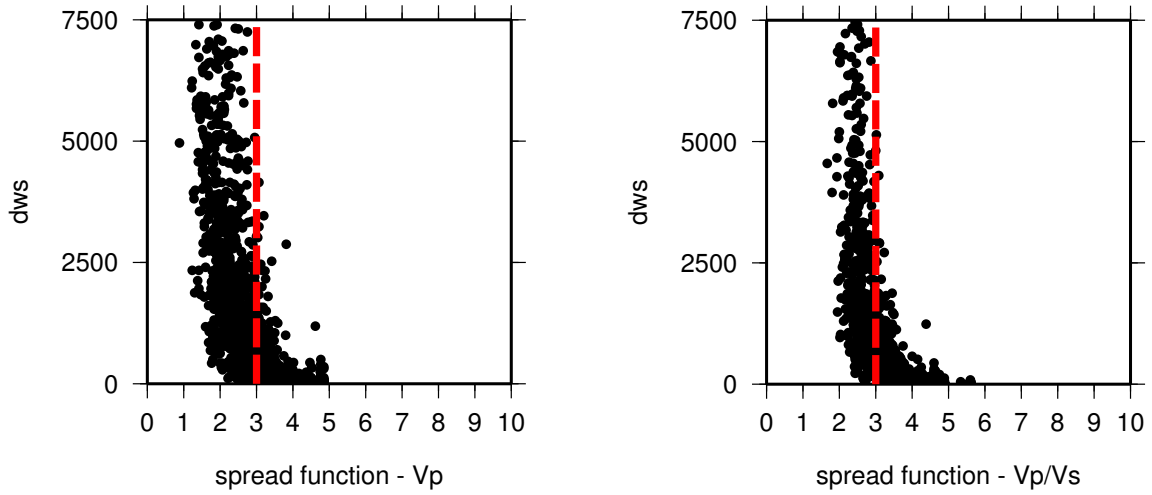


Figure 5.3: A plot of the DWS versus the spread function of the averaging vector of the model parameters for Vp and Vp/Vs models. The dashed line at SF=3.0 is the upper limit of values of the spread function values considered to be acceptable (see text for explanation).

Because the SF is computed by summing the contribution of all nodes, it gives no information on the directional properties of the parameter estimation (smearing). To analyze the smearing directions we contoured, for each node, the volume where the resolution is 70% of the diagonal element [Reyners et al., 1999].

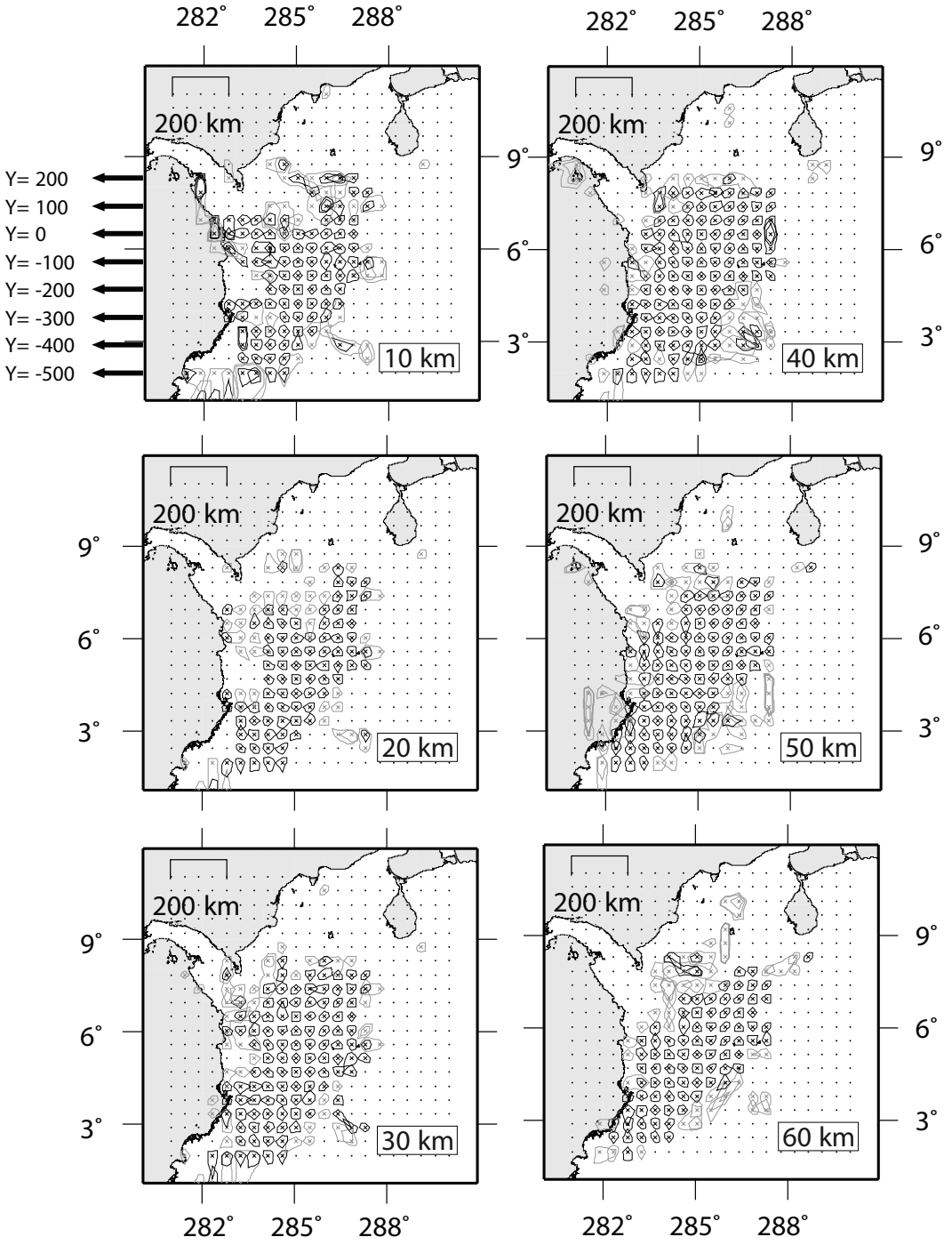


Figure 5.4: The 70% smearing contour for inverted nodes (crosses) with SF lower or equal to 3.0 in layers from 10 to 180 km depth for Vp model. The nodes with $SF < 1.5$ and $1.5 < SF < 3.0$ have black and gray crosses and contours, respectively. The black dots indicated the nodes not inverted or the inverted nodes with $SF > 3.0$ . The arrows on the top left panel on the right border indicate the eight W-E sections shown in Figure 5.5. The Y values are the offset distances of the sections from the center of the model. (Continued on the next page)

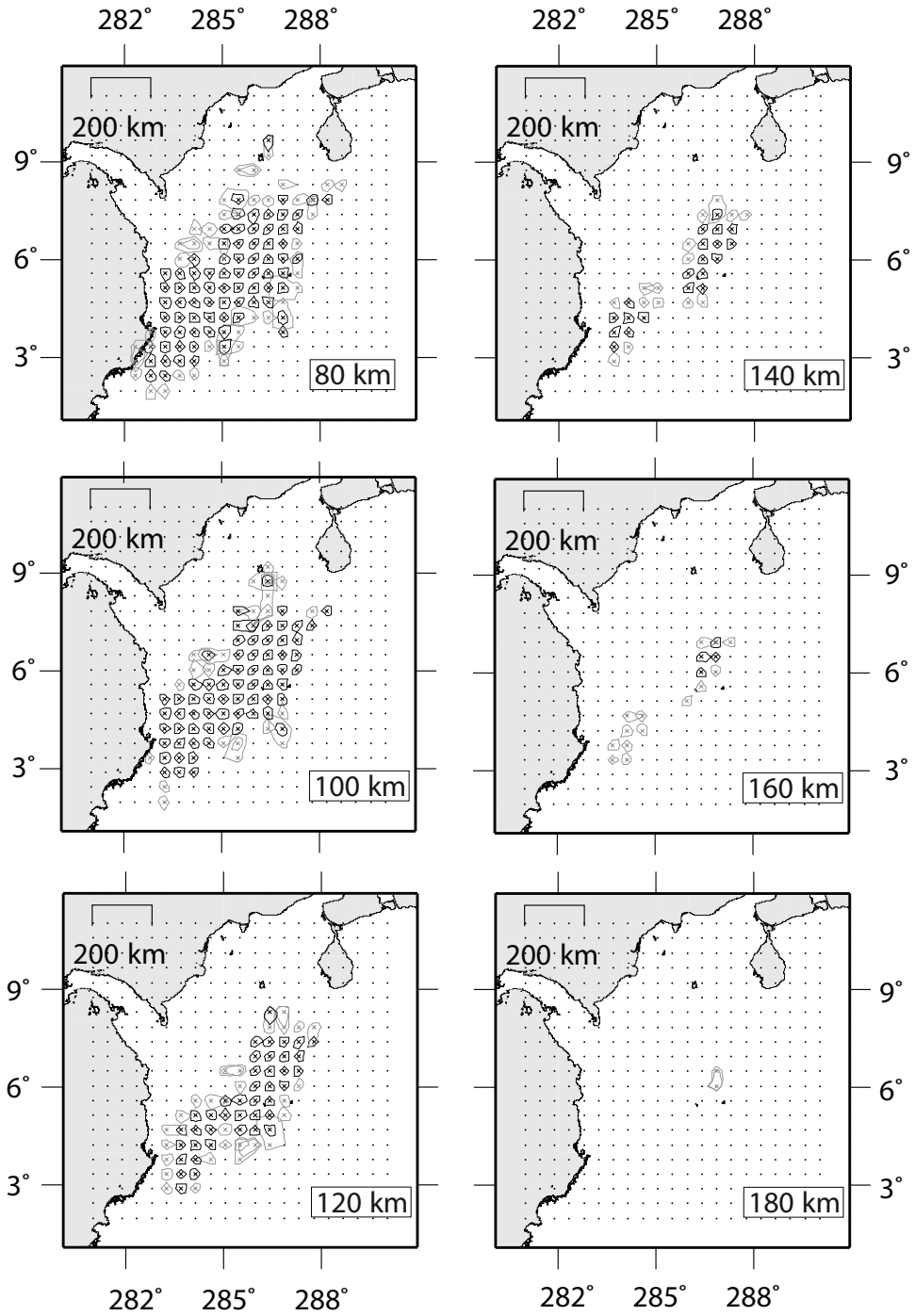


Figure 5.4: (Continued from previous page)

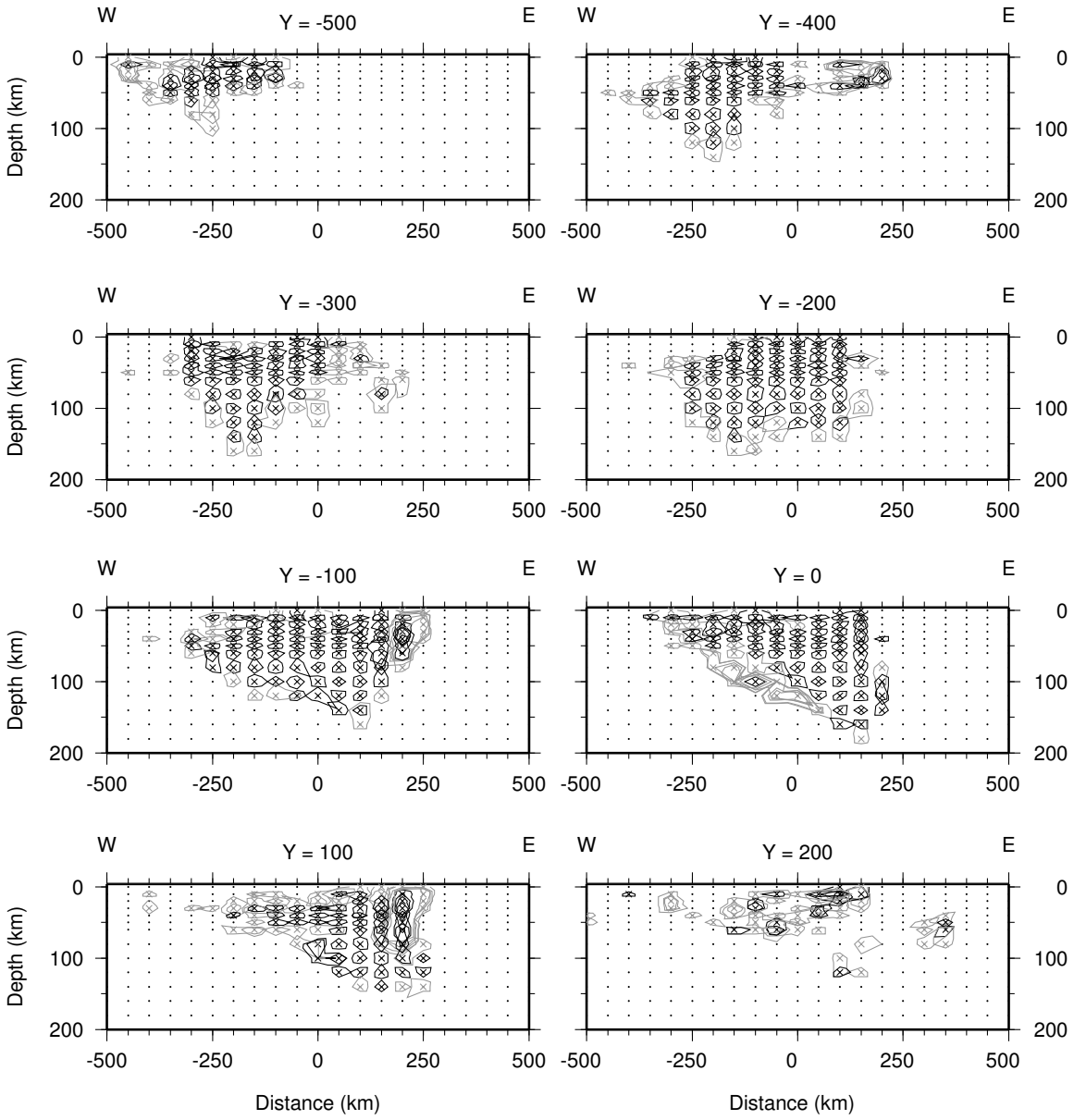


Figure 5.5: Same as Figure 5.4 but for eight vertical, W-E trending sections. Sections locations are shown in Figure 5.4, top left panel.

Figures 5.4 and 5.5 show the 70% smearing contour for nodes with SF $< 3$ in 12 inverted layers and in eight W-E trending vertical sections of Vp model. Well resolved nodes are characterized by low values of SF and smearing effects localized in the

surrounding nodes. I found that model parameters with SF$<$ 3 have good resolution, with only slight smearing of anomalies over adjacent nodes. The resolution within the study area is fairly good beneath the Eastern Cordillera and in the western Colombia, nearby the Pacific coast at crustal depth. Deeper layers show well resolved nodes (SF values $<$ 3) in the western Colombia, Eastern Cordillera and around the BN area. At 160 km depth the resolution is poor for most of the model. The only resolved area is in the nearby of BN. At 180 km depth, becouse of the substantial absence of seismicity, the resolution is insufficient and no resolved node is observed. In the vertical cross-sections (Y=0 and Y=100) a localized smearing effect is observed in the volume directly beneath BN, plausibly due to unidirectional ray-paths travelling westward from BN to the surface. In the northern part of the model (Y=200) few resolved nodes are observed, due to the poor station coverage. In summary, the resolution results good in the central and western-southwestern portion of the model. Northward from BN, and close to the Venezuela boundary, the resolution is poor.

### 5.2.1 Sensitivity tests

The solution quality was verified by sensitivity and resolution tests. The effect of the model grid spacing, dimensioning and distribution of the data on the imaging of structures can be tested with synthetic data. They can be designed on a priori geometries or on actual results: in both cases the aim is to check which parts and how many of the imposed anomalies can be restored given a 3-D grid and a station distribution. Another very common analysis consists of the checkerboard resolution test. In the checkerboard test, positive and negative anomalies are alternated in latitude

and longitude, and in depth. This simple alternation of positive and negative values becomes an image which is straightforward and easy to remember. Therefore, from the simple visual analysis of results and the comparison with the original distribution it is easy to understand where the resolution is poor and where it is good. The results of the checkerboard test give insights not only into which part of the model can be solved but also into the minimum and maximum size of the anomaly that can be resolved.

**Synthetic test**

Synthetic test were calculated using synthetic 3-D velocity models that mimics expected or a priori known real structures [Kissling et al., 2001]. The aim of the this test was to check how well the amplitudes of realistic velocity anomalies would be reproduced for a synthetic velocity model showing a similar subsurface structure as expected for the Colombia subduction zone (Figure 5.6, left column). A synthetic Vp model composed of both low and high Vp anomalies was created. I simulate a negative Vp anomaly (Vp = -10%) between 60 and 100 km depth located nearby the Pacific coast at 4°N - 5°N, and a positive Vp anomaly (Vp = +10%) elongated NE-SW and SW-dipping from 80 to 140 km, parallel to the strike of the Eastern Cordillera. Synthetic arrival times are generated, random noise added, and data are inverted using the same parameters as the real inversion. The negative anomaly is well recovered in all the layers except for the 60-80 km depth interval, where a smearing effect is observed and the recovered anomaly branches in various directions (Figure 5.6, right column).

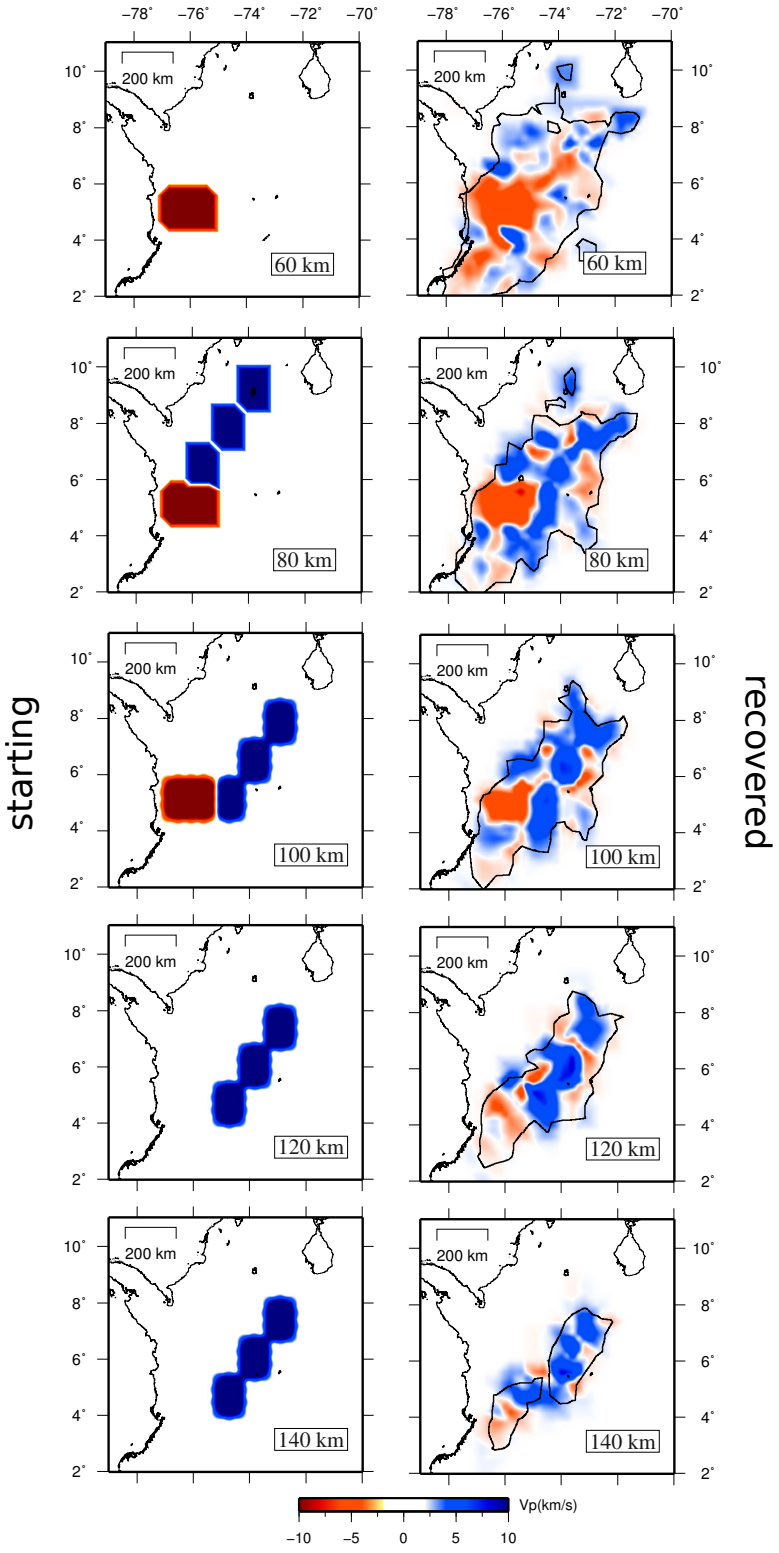


Figure 5.6: Assessment of solution quality by test with synthetic data. Left: synthetic input Vp model; right: recovered model after inversion. P-wave perturbations relative to 1-D initial reference model are shown. Horizontal layers are shown for different indicated depth. Black line outlines the best resolved region.

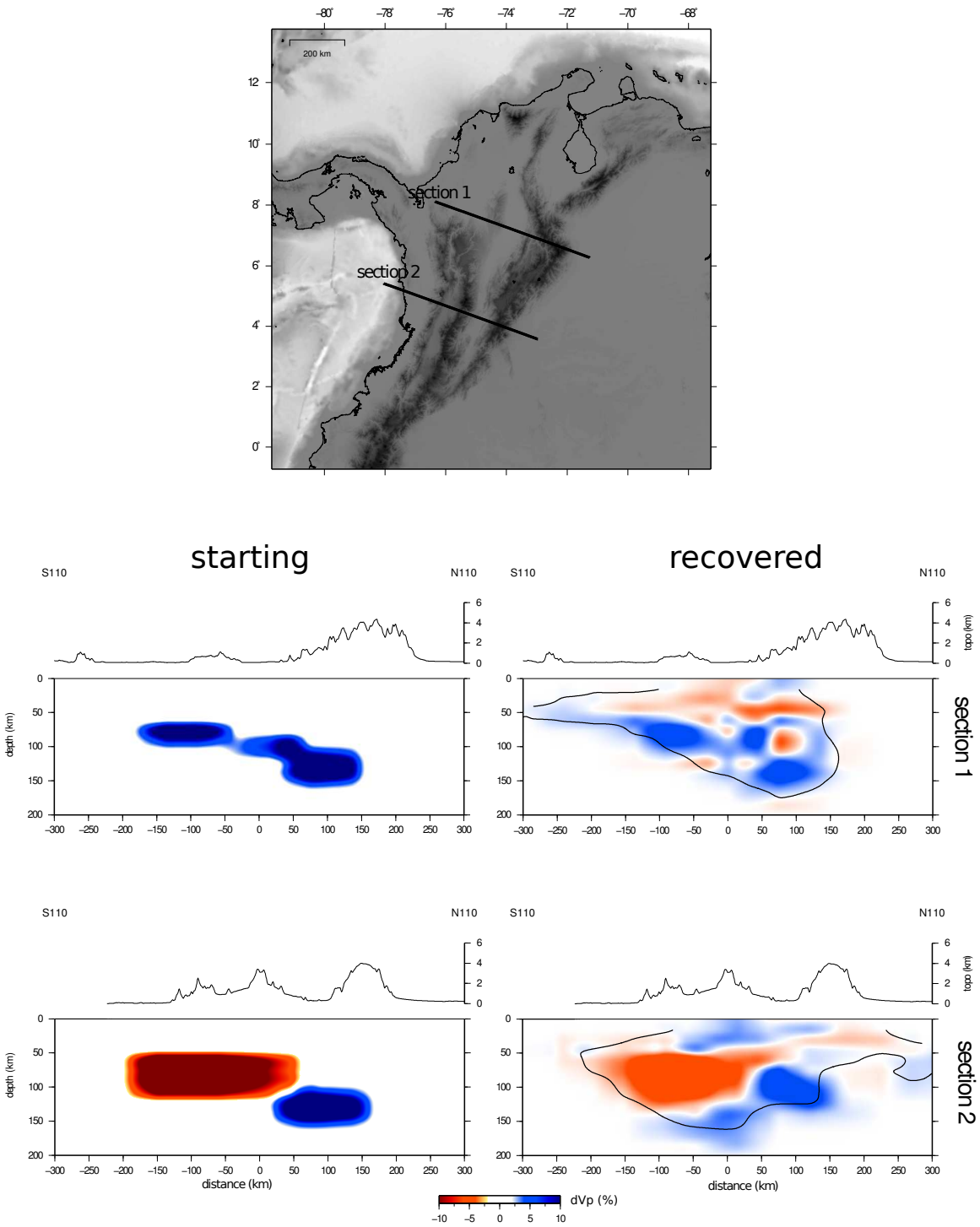


Figure 5.7: Same as Figure 5.6 for two vertical cross sections. The top panel indicates the traces of cross-sections. Black line outlines the best resolved region.

Furthermore, at this depth, the inversion produces slight artifacts of weak positive anomalies bounding the low-Vp. The recovered high-Vp anomaly in the 80 km depth layer shows a slight offset and mislocation with respect to the original position, while, in the remaining layers, the anomaly is fairly well reproduced. In the cross section shown in Figure 5.7, both the high-Vp and low-Vp anomalies are reproduced with good approximation.

Slight artifacts of bounding opposite anomalies are observed at 60-80 km depth around low-Vp, as previously described. Figures 5.6 and 5.7 show that the inversion procedure led us to recover an average of 60-70% amplitude of the starting model.

**Checkerboard test**

In the checkerboard test, I used positive and negative Vp anomalies of 5% alternated every two nodes in latitude and longitude, and every two layers in depth. Synthetic travel times were generated and inverted, after the addition of a gaussian noise with standard deviation equal to the final variance of the inversion, using a laterally homogeneous velocity model.

The results of the checkerboard test are shown in Figure 5.8. In the crustal layers (10-30 km depth), the inversion cannot reproduce the geometry and the amplitudes of the starting checkerboard anomalies. The geometry and arrangement of the recovered anomalies are quite different form the starting model except for the central area of the model. From 40 km depth, the recovered anomalies are fairly well reproduced in the central and western-southwestern Colombia. Despite the poor station coverage and the uneven distribution of seismicity, the recovering power of the tomographic

inversion is quite good between 50 km and 100 km depth. In this depth interval the checkerboard anomalies are reproduced with good fidelity both in shape and in amplitude. At 120 km depth the resolution is still good in the central Colombia, in the surrounding area of BN and partially, nearby the Pacific coast between 3°and 5°N. At 140-160 km depth recovered anomalies are observed only in the central area of the model.

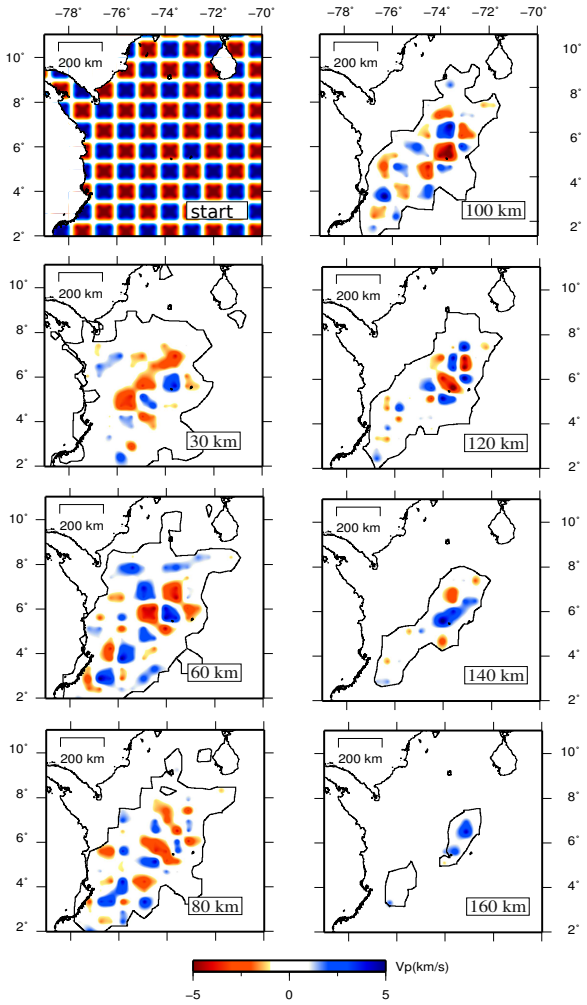


Figure 5.8: Checkerboard test. In the top left panel the Vp synthetic starting model is reported; in the remaining panels the models restored by the tomography for some layers at different depth are displayed. The black line outlined the best resolve region of the model (SF< 3).

## 5.3 Results

The tomographic results are presented in the form of horizontal layers (Figure 5.9) and vertical cross-sections (Figure 5.10). The figures show P-wave and Vp/Vs ratio perturbation relative to the 1D reference model. Velocity perturbation were preferred to the absolute values, being easier to interpretate. Hypocentral locations are shown for each horizontal layer within 10 km perpendicular to profile. In the vertical sections hypocentres are projected into the sections within 50 km perpendicolar to profile. The tomographic models reflect the complexity of the subduction dynamics beneath Colombian Andes. The tomographic images (in particular the horizontal layers) often show complicated Vp and Vp/Vs patterns, making the interpretation quite difficult. To avoid misinterpretations I focused my description only on the more relevants and well constrained features. Given the large reading errors affecting the S-picks (see Chapter 4), I used the Vp/Vs model only to facilitate the interpretation of the more robust Vp model.

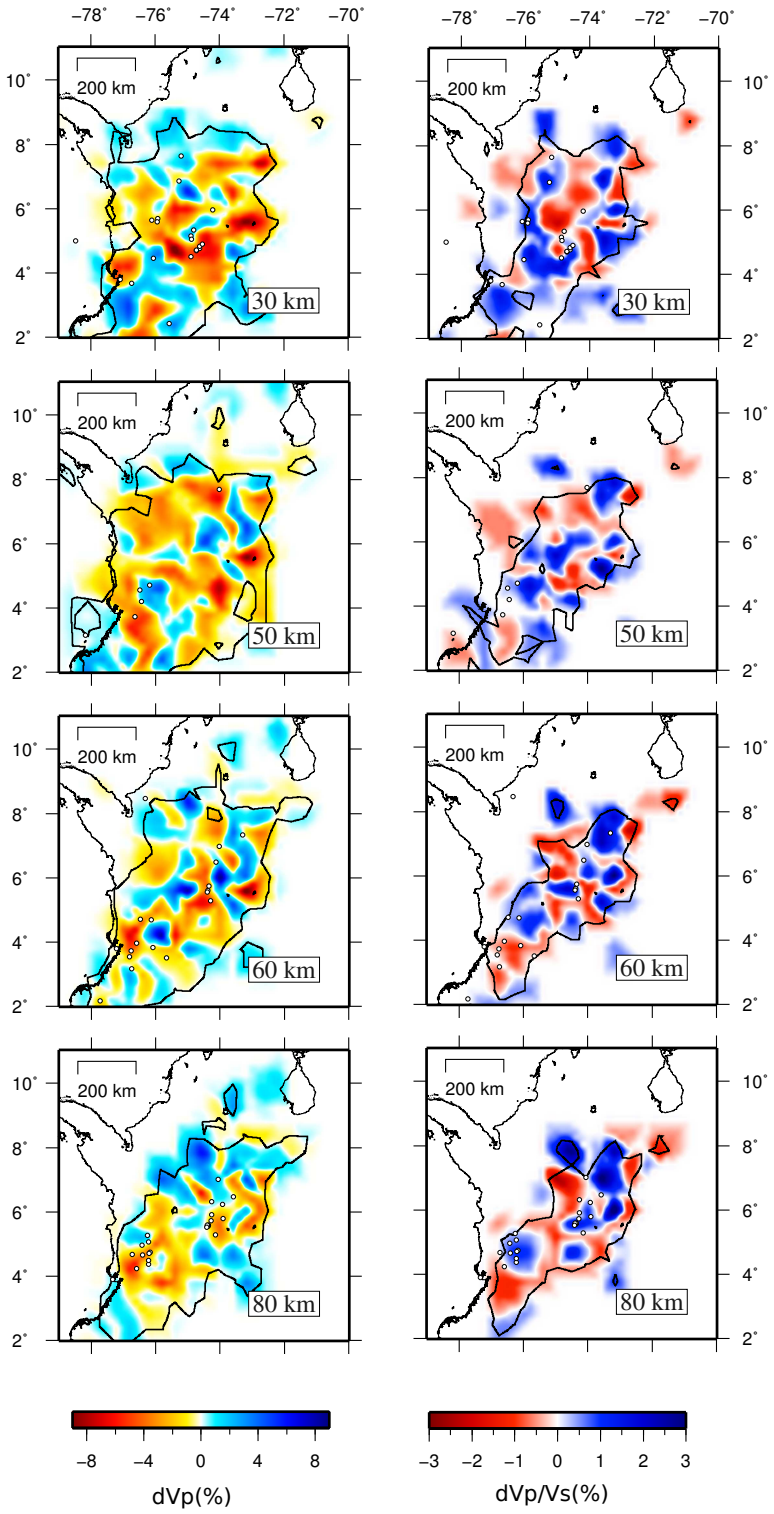


Figure 5.9: Velocity perturbation relative to initial 1-D model in a selection of the inverted layers of the tomographic model. The black line outlines the limits of the resolved region where the SF 3.0 In each layer, I plotted the relocated seismicity occurring 10 km above and below the layer. (Continued on the next page)

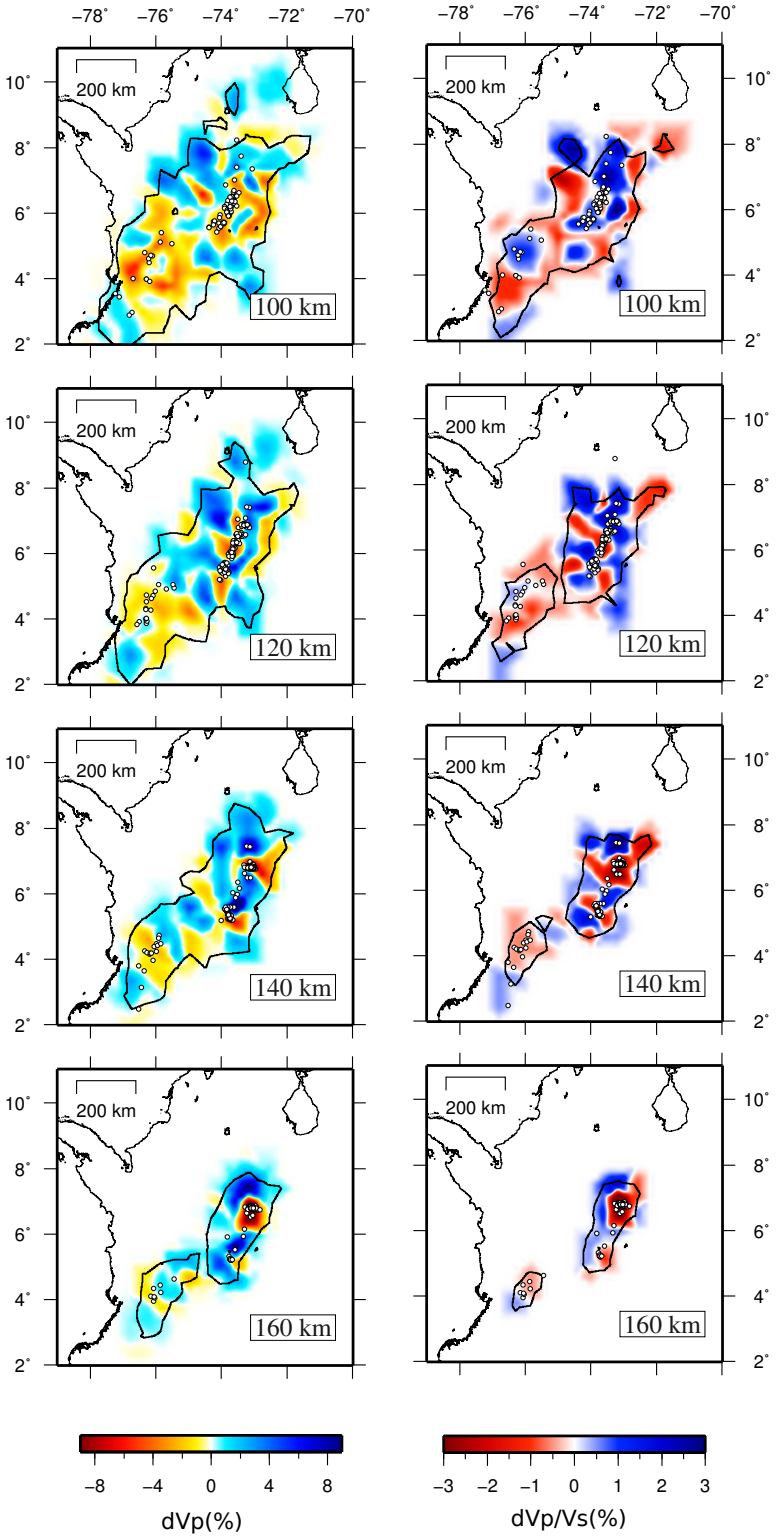


Figure 5.9: (Continued from the previous page)

### 5.3.1 Horizontal layers

- Crustal layers. At crustal depths Vp and Vp/Vs models show complicated patterns, plausibly resulting from the structural complexity of the Andean belt. In these horizontal layers it is difficult to distinguish relevant tectonic features. Here I show only the 30 km depth layer. The main features are the presence of a localized low-Vp anomaly (Vp -5%) nearby the Pacific coast around 4°N, where a cluster of shallow seismicity is observed. Such feature can also be found in the deeper layers, to a depth of 100 km. The Vp/Vs model shows a bipartition: beneath the Eastern Cordillera a diffuse low Vp/Vs is observed; South of 5°N the model shows high Vp/Vs ratio along strike of the Cordilleras.

- 50-80 km depth layers. Within this depth interval the more relevant features are represented by the low-Vp zone (Vp -4%) which is mostly concentrated in the area nearby the Pacific coast with increasing depth, at around 4°N. Here is located part of the seismicity occurring in the Pacific coast area. The Vp/Vs ratio show, in general, diffuse high values beneath the Eastern Cordillera and, more localized, in correspondence of the low-Vp zone.

- 100-140 depth layers. In this depth range the tomographic models become more distinguishables and can be divided in two zones. (1) The Bucaramanga area is mostly dominated by high-Vp and high Vp/Vs anomalies. Narrow low-Vp zones, elongated along strike of the Eastern Cordillera, can be observed. Here the relocated seismicity is located in both positive and negative Vp anomalies. (2) Nearby the Pacific coast, between 5°and 3°N, a diffuse low-Vp anomaly can

be detected. Most of the seismicity occurring in this area is located within the low-Vp zone. At 100 km depth the Vp/Vs model show high value localized in between 4N and 5°N, and a low value more southerly. For greater depths the Vp/Vs model show poor resolution in this area.

- 160 depth layer. At 160 km depth the most prominent feature is represented by the BN which is located well inside a marked and localized low-Vp anomaly (-10%) and low Vp/Vs anomaly (-3%). The remaining Eastern Cordillera seismicity is located in a high-Vp area. At this depth, the velocity pattern nearby the Pacific coast presents weak and poor resolved anomalies and will be described more carefully in the vertical cross-sections. The Vp/Vs model is poorly resolved and cannot be discussed.

### 5.3.2 Vertical cross-sections

In the followings I describe in detail three vertical cross-sections located in "key-areas" of the tomographic model. The azimuth of the cross-section was choosen after careful examination of the tomographic model. In particular I verified the presence of a flatly-dipping Vp anomaly oriented northward indicating a possible Caribbean dipping plate feature, in NS oriented sections (not shown here). In none of these sections it is possible to find such a feature, being the model very poorly resolved towards the Caribbean coast and Venezuela. In this dataset clear evidence for the Caribbean Wadati-Benioff plane is lacking. The choosen azimuth (N110) allow to interpretate the cross-section almost perpendicularly to the main tectonic elements and seismicity (Figure 5.10).

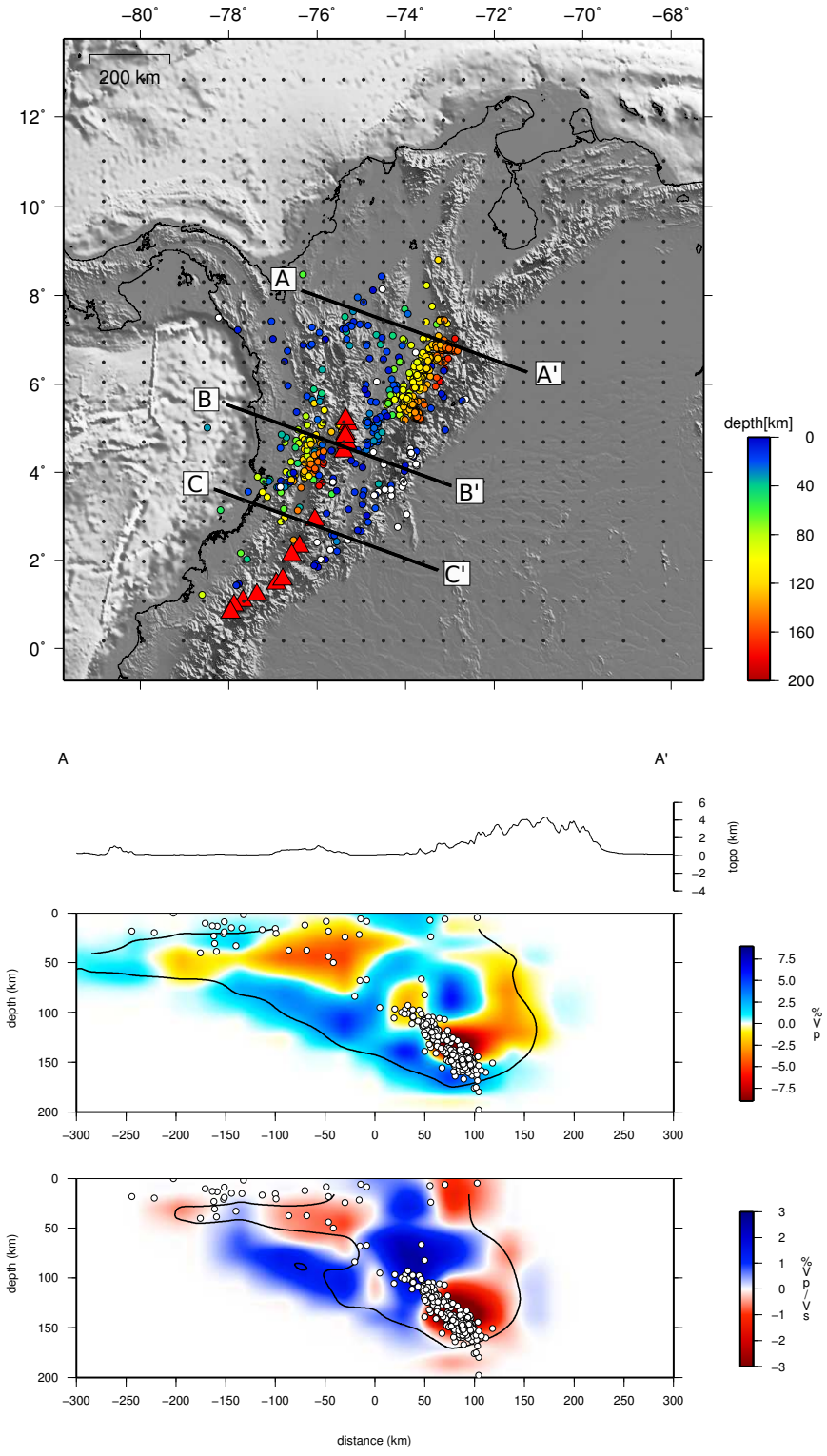


Figure 5.10: Vertical sections of the tomographic model. In the top panel the locations of the cross sections, earthquakes and grid nodes used in the inversion are shown in map. The black lines indicate the limit of the resolved volume (SF $< 3$). The earthquakes (white circles) are projected into the cross section in a 100 km-wide band. (Continued on the next page)

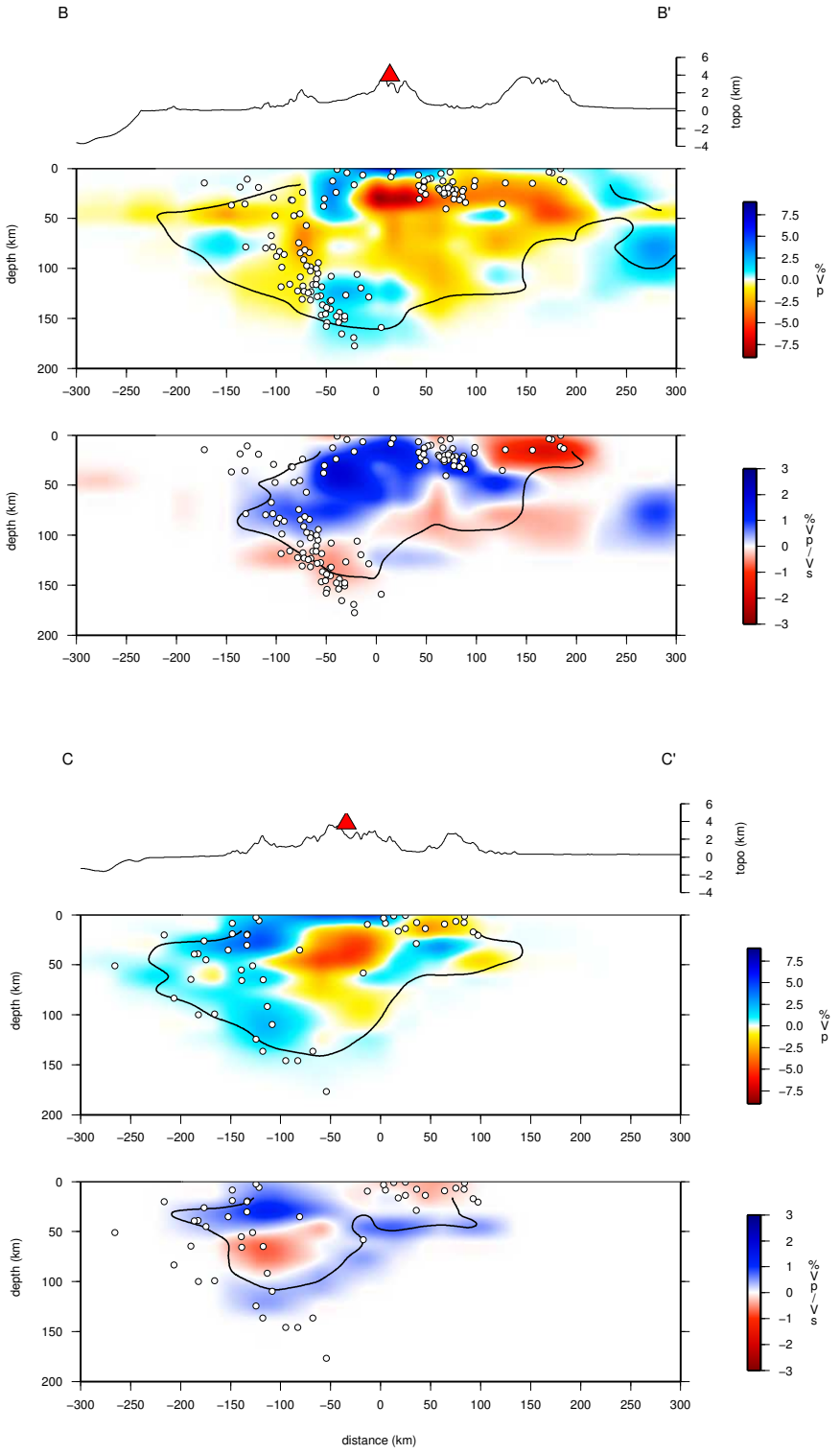


Figure 5.10: (Continued from the previous page)

- Profile A-A' lies in the BN area. The most notable feature is the location of the seismicity of the nest in a strong low-Vp anomaly (Vp -10%). The seismicity prolongates updip towards the surface delineating a Wadati-Benioff zone dipping roughly south-eastward, while the low-Vp anomaly is not continous and is interrupted between 70 and 100 km depth. Beneath the seismicity and parallel to the low-Vp anomaly, a continuous positive anomaly can be observed to a depth of 60 km depth, where the dip of high-Vp slightly changes and the anomaly flattens. The Vp/Vs ratio although less resolved than Vp model, shows that the bulk of the BN seismicity lies in a negative anomaly (-3%). A positive high Vp/Vs (+3%) can be observed directly above the termination of the seismicity plane in the range between 60 and 100 km depth.

- Profile B-B' is centered in the volcanic area at 5°N. The prominent feature is a low-Vp anomaly in the area of Pacific coast to a depth of 130 km (Vp -3%). Below this depth a high-Vp anomaly is observed. The seismicity delineates a Wadati-Benioff zone 45°E-SE dipping and is located within the low-Vp volume to a depth of 120 km and within high-Vp anomaly at deeper depths. Below 110 km depth the seismicity appears more concentrated, in a zone with a low Vp/Vs ratio. A negative Vp (-7%) and positive Vp/Vs anomaly (+3%) can be observed at shallow depth (20-60 km). The former is centered directly below the volcanic area whilst the latter shows a more complicate pattern and it branches from Wadati-Benioff zone to a shallow depth, below the volcanoes.

  The low-Vp picture of a Wadati-Benioff zone shown in this cross section is rather different from the classically imaged high-Vp dense and cold seismically active,

slab. However Husen et al. [2003] showed a similar velocity pattern in Costa Rica by relating the low-Vp body to the age, thickness and thermal state of the downgoing Cocos plate. The Vp pattern observed in this cross-section can be related to the subduction of relatevly hot and young segment of Nazca plate.

- Profile C-C' lies in the southernmost part of the resolved model, nearby the Pacific coast (Figure 5.10). The Vp/Vs model is poorly resolved and will be not discussed. The Vp model shows a positive Vp anomaly (+5%) dipping eastward-southeastward. The seismicity, although poor, lies within the high-Vp anomaly, delineating a classical Wadati-Benioff zone related to the steep subduction of the Nazca plate. Above the Wadati-Benioff zone a low-Vp anomaly (Vp -5%) can be seen, from 80 km to crustal depth overlain in the surface by a volcanic area.

# Chapter 6

# Discussion

## 6.1 Effect of the heterogeneity of the Nazca plate on subduction dynamics

The regional pattern of seismicity and volcanism shows a high degree of segmentation along strike of the Andean belt. Segments of steep slab subduction alternate with aseismic regions and segments of flat slab subduction [Isacks, 1988; Gephart, 1994; Gutscher et al., 1999, 2000a] (Figure 6.1). This segmentation is related to the heterogeneity on the subducting Nazca Plate [Gutscher et al., 1999; Gailler et al., 2007; Jordan et al., 1983; Hall and Wood, 1985; Sillitoe, 1974]. In general, tectonics above flat subduction segments show no significant magmatism [McCann et al., 1979; McGeary et al., 1985]. In some cases (e.g. Perù, Panama) an intermediate depth seismic gap is observed.

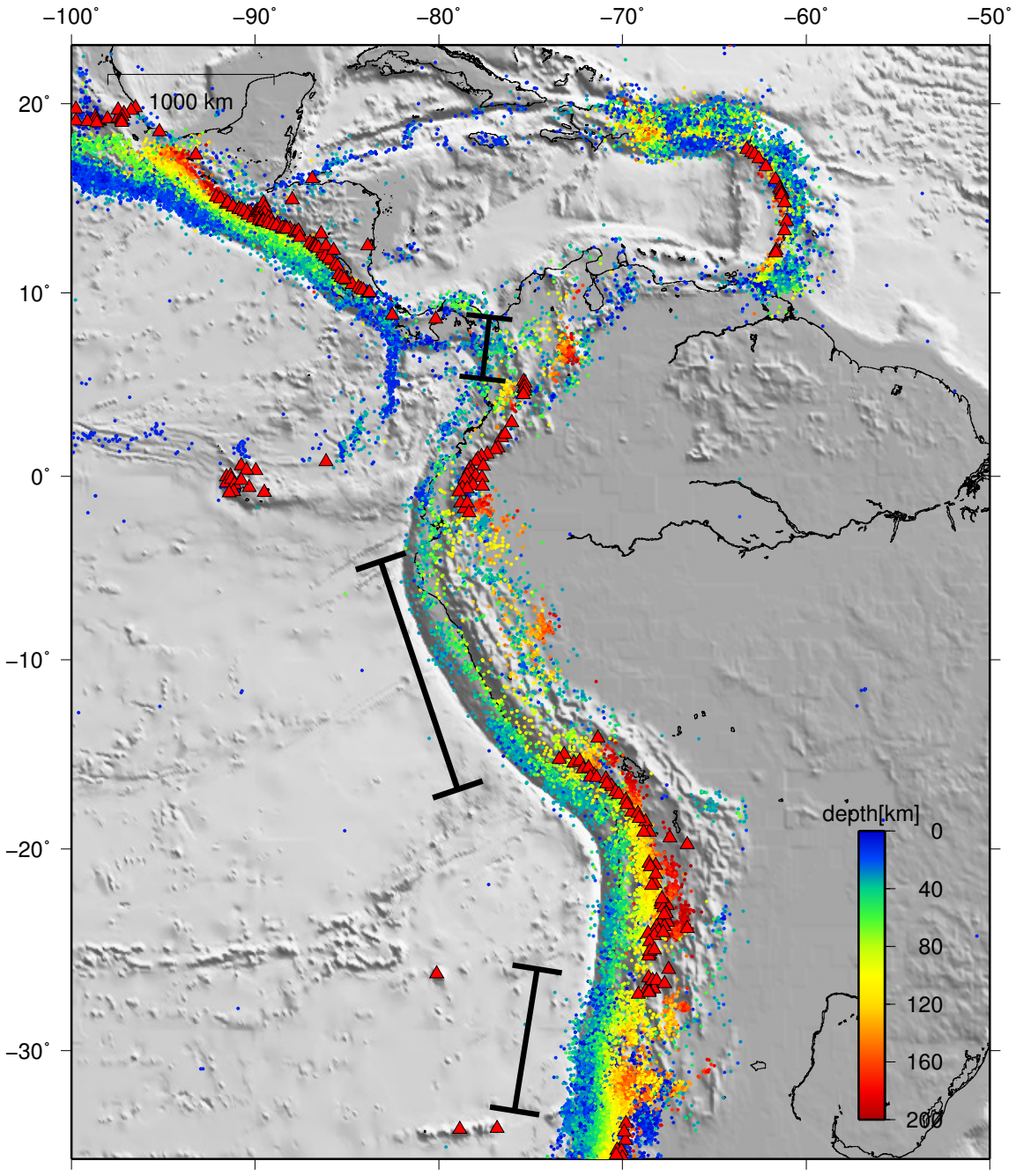


Figure 6.1: Seismicity and volcanism in Southern and Central America. Earthquakes with M> 3.5 recorded in the time period 1993-2009 are shown. The ipocentral locations has been downloaded from National Earthquake Information Center website (NEIC - http://earthquake.usgs.gov/regional/neic/). Red triangles represent volcanoes. Volcanic gaps are indicated by black segments.

## 6.2 Northern Andean margin

The tectonic segmentation of northern Andean margin has been well documented by several works [Gutscher et al., 1999, 2000b; Gailler et al., 2007]. Seismicity and volcanism are not continous and largely inhomogeneous [Gutscher et al., 1999]. According to Gutscher et al. [1999] such tectonic assembly, in Southern Colombia and Ecuador, is a direct consequence of the heterogeneity and the segmentation of the downgoing Nazca plate, related to the presence of several slab tears and the subduction process of the Carnegie ridge between 0°and 2°S. The joint analysis and interpretation of relocated seismicity and tomographic results obtained in this study allows to invoke a similar mechanism for the central and northern Colombian Andes. In Colombia the volcanic chains are all located south of 5°N and overlie the steeply dipping part of the Nazca slab. North of 5°N volcanism disappears and the seismicity rate strongly increases beneath the Eastern Cordillera.

To understand the dynamics of subduction beneath Colombian Andes, it is useful to briefly summarize the tectonic evolution of Nazca plate off the Pacific coast of Colombia as reported by Sallares and Charvis [2003]. The formation of Cocos-Nazca plate took place around 25 Ma when the Farallon plate was subdivided into Cocos-Nazca plate (south) and the Juan de Fuca plate (north) [Hey, 1977]. Because of the differential stresses between the northeastward subducting Cocos segment and the eastward subducting Nazca segment, rifting was initiated at about 23 Ma between both segments near the Galapagos hot spot, evolving later into N-S seafloor spreading along the Cocos-Nazca Spreading Center (CNS) and originating both Nazca and Cocos plates [Hey, 1977; Lonsdale and Klitgord, 1978]. The V-shaped Carnegie and

Cocos Ridges outline the motion of the Galapagos hotspot over the east trending Nazca plate and the northeast trending Cocos plate, respectively [Pennington, 1981; Kolarsky et al., 1995]. Carnegie and Cocos Ridges separated from one another during a continuous period of rifting and seafloor spreading between 23 and 9 Ma [Hey, 1977; Lonsdale and Klitgord, 1978]. Kinematic reconstructions suggest that the Malpelo Ridge is a former continuation of the Cocos Ridge, which was split by dextral motion along the N-S trending Panama Fracture Zone (PFZ). This fracture zone initiated at about 9 Ma, as a consequence of the blocking of the Cocos plate subduction beneath Middle America [Sallares and Charvis, 2003]. Hence, from 9 Ma to the present, N-S seafloor spreading has continued between the Cocos and Carnegie Ridges west of the PFZ, but not along the eastern segment [Hey, 1977; Pennington, 1981]. Motion along the PFZ is also suggested to have induced N-S extensional stresses in the northeastern part of the Nazca plate, resulting in the separation of the original Malpelo Ridge into several smaller ridges (current Malpelo, Regina, and Coiba). The initial rift would have evolved later into the currently E-W trending Coiba transform fault (CTF) [Lonsdale and Klitgord, 1978], so the small block located between Coiba transform fault to the south, Panama to the north, Colombian trench to the east, and PFZ to the west may be interpreted at present as an independent microplate (Figure 6.2). Other authors [De Boer et al., 1988; Lonsdale, 2005] refer to this tectonic element as the Sandra Ridge. The Harvard CMT catalog shows left lateral strike slip motion along the Sandra ridge-CTF. Hereinafter I refer to this element as CTF. Both active and extinct rifts of the CNS as well as fracture zones and transform faults are expressed in the bathymetry (Figure 6.2). The age of the Cocos Ridge subducting at

the trench is 14–15 Ma based on radiometric data [Hoernle et al., 2002], and the ages of Carnegie Ridge at the trench and the conjugate Malpelo Ridge are estimated to be 20 Ma from magnetic anomalies reconstruction (e.g., Lonsdale and Klitgord [1978]).

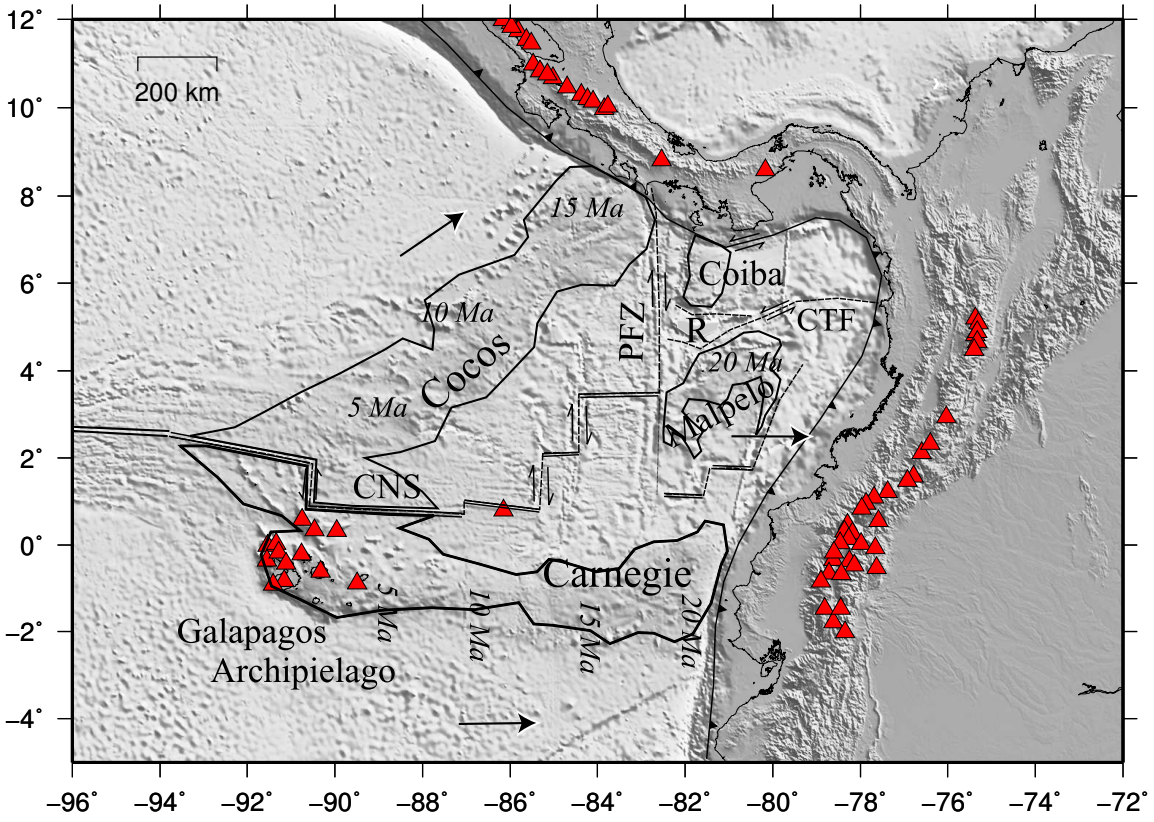


Figure 6.2: Schematic tectonic map of North West South America. The the most prominent geological and tectonic features, and the estimates of lithospheric age based on absolute plate motions are shown. Arrows indicate the relative plate motions DeMets et al. [1990]. CTF, Coiba Transform Fault; CNS,: Cocos-Nazca Spreading Center; GFZ, Grijalva Fracture Zone; PFZ, Panama Fracture Zone; R, Regina Ridge; YG, Yaquina Graben. Seafloor ages are based on reconstruction of magnetic anomalies [Lonsdale and Klitgord, 1978]. Modified from Sallares and Charvis [2003]

## 6.3 Colombian Andes

The distribution of seismicity and the tomographic model calculated in this study give new insights into the dynamics of subduction beneath the Andean belt of Colombia. To better understand the geometries of the subducting system a subset of 5947 earthquakes were relocated with 3D tomographic model and plotted in map and in cross-sections in Figures 6.3 and 6.4. The seismogenic zone and slab geometry of Colombia exhibit significant spatial variation corresponding to the spatial change of the incoming plate. The study area covers three sectors (Figure 6.3) which can be characterized in terms of the geometry of seismicity patterns and P-wave velocity structure as follows:

- Sector 1: Bucaramanga - Eastern Cordillera (North of 5°N)

  The volcanically inactive sector north of 5°N is inferred to be a flat-subducting segment of the northernmost part of the Nazca plate. The absence of volcanism often characterizes flat subduction environments [McGeary et al., 1985]. The tomographic model clearly shows a flatly and low-Vp Wadati-Benioff zone underlain by high-Vp (Figure 6.3). Even if dipping seismicity of the Eastern Cordillera-Bucaramanga area is far from the westerly Pacific trench (about 500 km), the tomographic model and relocated earthquakes show the continuity of a flatly slab north of 5°N from the Eastern Cordillera westward to the trench (Figures 6.3 and 6.4). A similar seismicity distribution was documented by Taboada et al. [2000], but they referred the deep Eastern Cordillera seismicity to the Caribbean slab. Zarifi et al. [2007] describe two slabs north and south of Bucaramanga nest, the northern one being associated with the Caribbean Plate.

They also state that the "southern slab" clearly differs from the Nazca slab, but they do not explain its nature and origin. Linking this sector to the subduction of Caribbean or Paleo-Caribbean plate [Taboada et al., 2000] is not reasonable, given the Vp pattern anomalies and the seismicity distribution elongated almost NNE (the more northerly Caribbean trench, if existing, is expected to present tectonic structures oriented mostly E-W). The 200 km cut-off seismicity depth can be interpreted in two ways: either it corresponds to the leading edge of the subducting slab, or it represents the depth at which aseismic deformation occurs within a much deeper slab. However, the three stations of Trenkamp et al. [2002] located on the Western-Central Cordillera between 5°N and 7°N (BHSL, MZAL, and RION) consistently yield 13.2 to 18.5 mm/yr velocity vectors directed N74°to N80°with respect to stable South America. Such velocity field translates into 9.2 to 13.1 mm/yr (average 11.1 mm/yr) components orthogonal to the N110°trend of the Wadati- Benioff plane beneath the Eastern Cordillera. Extrapolating such present velocity field to 15 Ma (main Andean tectonic phase in the Eastern Cordillera), I get a 166 km orogen-normal shortening, which compares (considering incertitude on both GPS data and subduction onset age) to the 140 km long slab retrievable by seismic data. This suggests that seismicity cut-off does correspond to the leading edge of the subducting slab, and that subduction rate has remained rather constant since mid Miocene.

- Sector 2: Pacific coast - between 3°N and 5°N.

South of 5°N, a completely different pattern of volcanism and seismicity is observed with respect to sector 1. The seismicity clearly delineates a steep

Nazca Wadati-Benioff zone, lying mostly on a low-Vp anomaly; a volcanic chain (Nevado del Ruiz, Romeral, Cerro Bravo among others) is present. The seismicity rely on a low-velociy zone to a the depth of 120-130 km (Figure 6.3 6.4), suggesting here the subduction of a warm Nazca plate. A similar Vp pattern was found by Husen et al. [2003] in central and southern Costa Rica (for shallower depth), confirming that the subduction of a young oceanic lithosphere produces tomographic images rather differents from the classical high-Vp dipping slab.

- Sector 3: Pacific coast - Between 2°and 3°N.

  Even if on the edge of well-resolved region of tomographic model, a further segment can be identified south of 3°N. As shown in Figure 6.3, here the tomographic model displays a different pattern of Vp, with respect to the sectors 1 and 2. The volcanism are poorly represented and the seismicity of the Wadati-Benioff zone, although poor, relies on a weak high-Vp anomaly (Figures 6.3 and 6.4), suggesting the subduction of a cold and dense segment of Nazca plate.

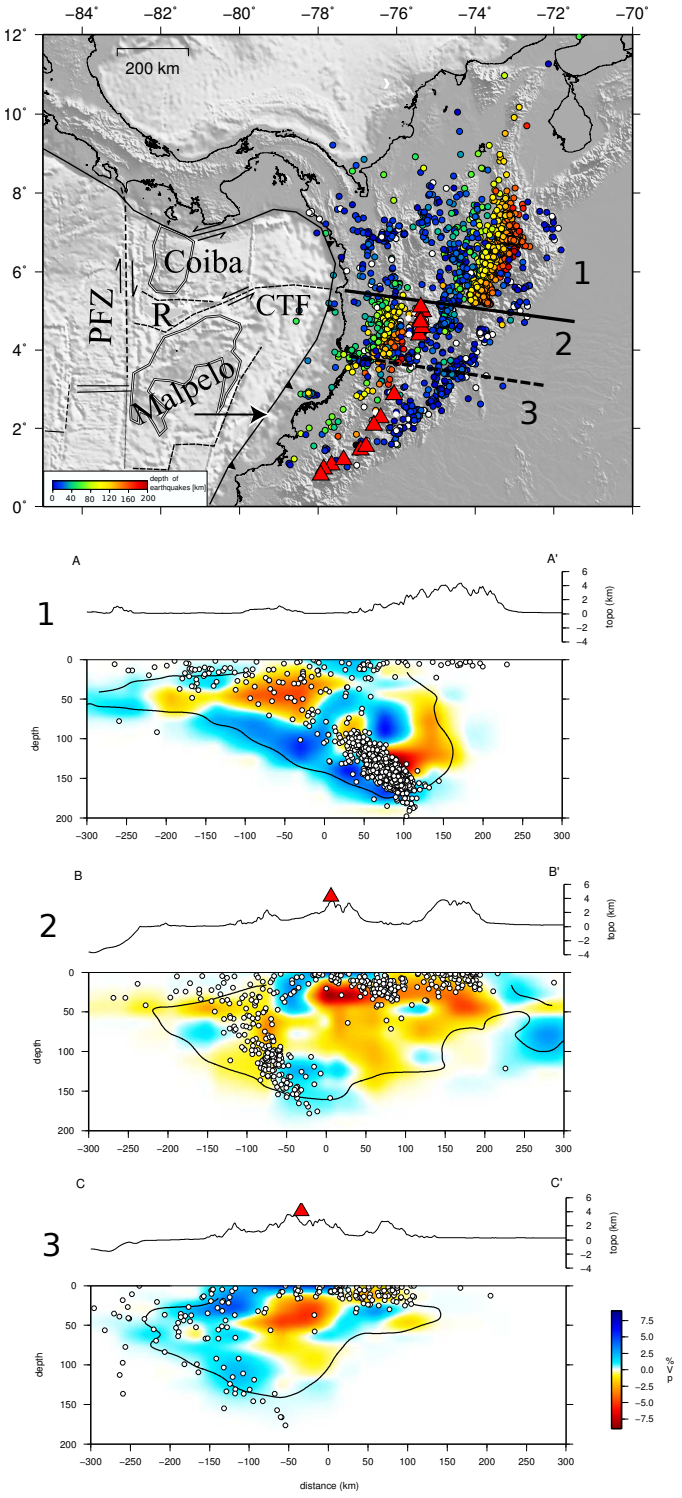


Figure 6.3: In map a subset of 5947 earthquakes relocated with tomographic model are plotted. Tomographic cross sections with relocated seismicity are shown. Cross sections location are indicate in Figure 5.10. Thich black solid line indicates the inferred slab tear at 5°N. Black dashed line indicates a possible slab tear at 3°N (see text for explanation). Labels as in Figure 6.2. The numeration (1,2,3) indicates the three sectors described in the text.

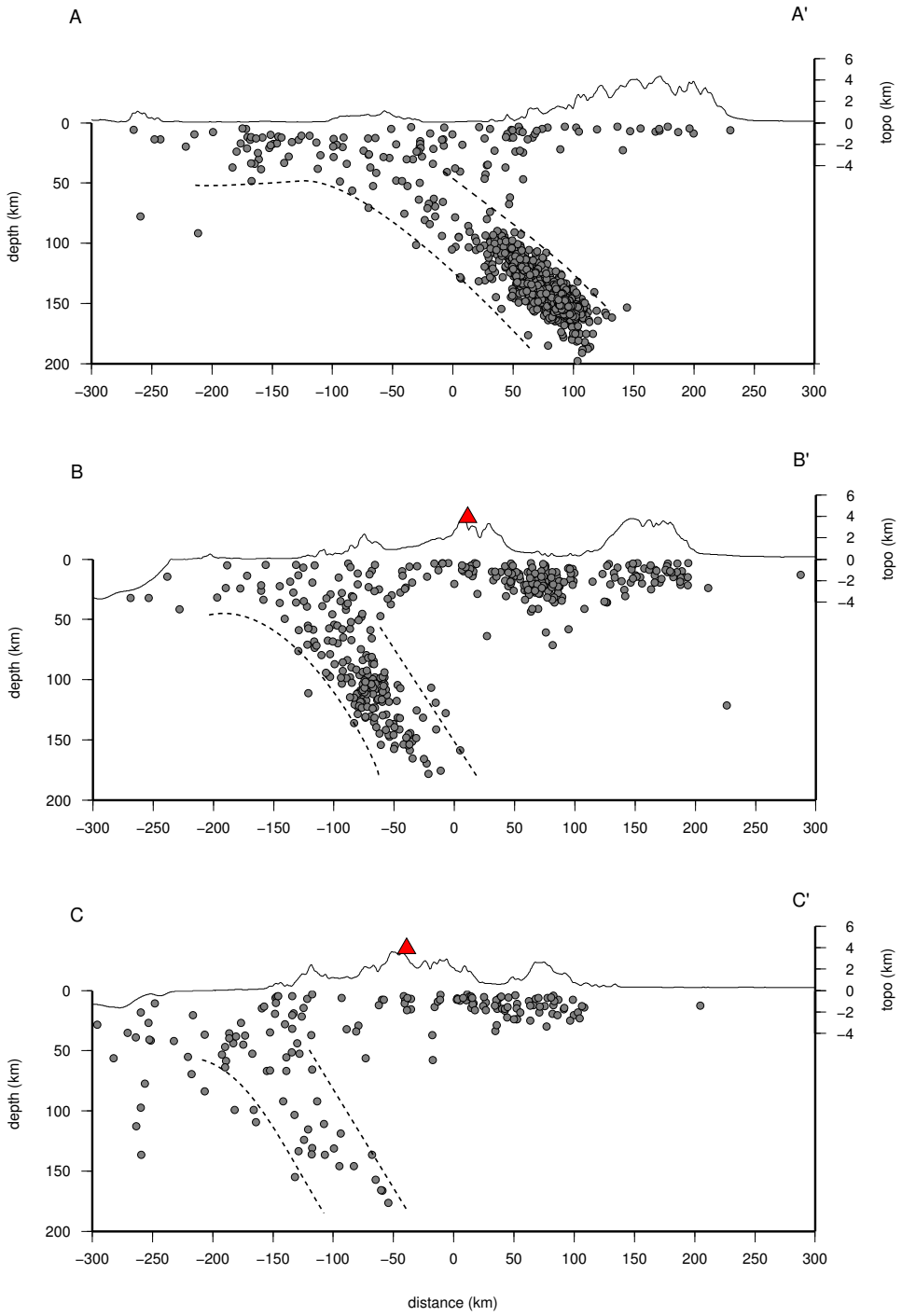


Figure 6.4: Vertical cross-sections showing the relocated seismicity. The Wadati-Benioff zone is outlined with dashed lines. Red triangles represent volcanoes. Relocate seismicity is projected in the sections in a 100 km wide band. Cross sections locations are indicate in Figure 5.10

In general, subducting oceanic slabs are imaged by seismic tomography as high-Vp features [Zhao et al., 1995; Reyners, 1998; Husen et al., 2000; Zhao, 2004; Nakajima et al., 2001]. After formation, mid-ocean ridge lithosphere cools and thickens until it is subducted. Subduction rates are generally faster than thermal diffusion, yielding a cold core within the subducting slab and a strong temperature gradient across the interface between the subducting plate and the overlying plate [Husen et al., 2003]. The temperature difference between the cold slab and the warm surrounding mantle depends mainly on the age of the subducting plate and the subduction rate. The older the plate and the faster the subduction, the colder the subducting slab. The colder the slab, the higher the velocity difference between the subducting slab and the surrounding plate. Often local tomography study cannot image a low-velocity zone on top of the high-velocity slab because the vertical depth resolution is poor [Protti et al., 1996; Graeber and Asch, 1999]. In some cases the top of the subducting slab is a priori defined by a high-velocity first-order discontinuity [Zhao et al., 1992, 1995; Nakajima et al., 2001]. In Colombia the complex lithospheric structure of the down-going plate produces "anomalous" tomographic images, suggesting that subduction environments could be much complicated and the simple picture of a cold, dense, high-Vp subducting slab is oversimplified [Husen et al., 2003]. As described above, the E-SE subducting Nazca plate presents strong variations, mostly latitudinal, with presence of rift, volcanic ridge and transform faults, the most oriented E-W, in the Panama Basin. Such a structural complexity may results from the presence of inherited structure related to the breakup of the Farallon plate started 25 Ma, occurred in the area of the actual Panama Basin (Figure 6.5).

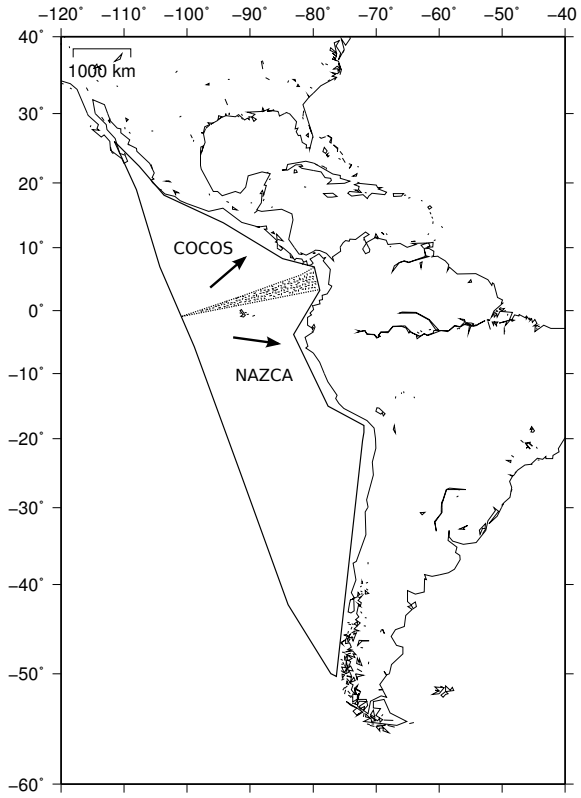


Figure 6.5: Fragmentation of the Farallon Plate into the Cocos and Nazca plates. Forces pulling the plate towards the trench are indicated by arrows. Modified from Wortel [1984]

The seismicity distribution and Vp pattern observed in the sectors 1, 2 and 3 suggests that the the complexity and heterogeneity of the Nazca plate, described in the previous section, may influence the subduction dynamics. The abrupt offset in seismicity at 5°N can be referred to a slab tear oriented roughly East-West (Figure 6.3 and 6.6). This slab tear is collinear to the CTF and separates the northernmost portion of the Nazca plate, the indipendent Coiba microplate [Sallares and Charvis, 2003]. I postulate that the CTF evolved into the slab tear once the Coiba microplate began subducting. A similar mechanism was proposed by Vargas [2011]. The Figure 6.6 shows the distribution of the relocated seismicity along the strike of the East-

ern Cordillera. The cross section is centered at 5N. The presence of a slab tear is marked by the abrupt change in seismicity rate in the central part of the cross section.

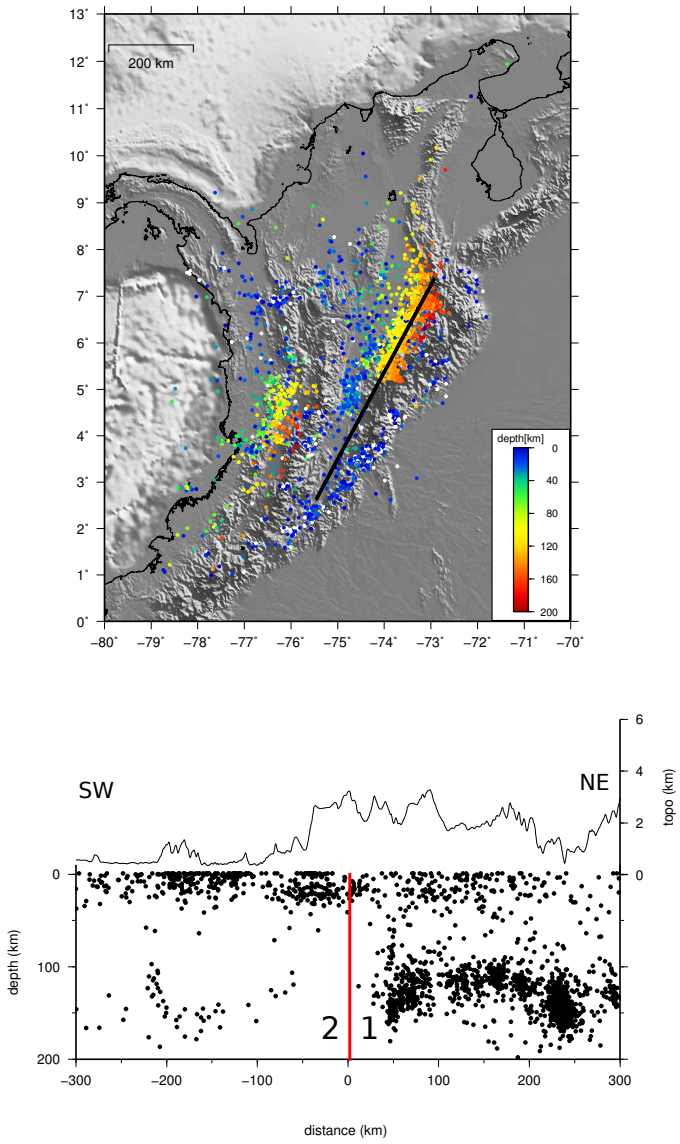


Figure 6.6: Vertical cross-section along strike of the Eastern Cordillera. Location of the cross-section is shown in the map. Relocate earthquakes are shown in map and projected in a band wide 300 km in the cross section. Red vertical line indicates the inferred slab tear separating sectors 1 and 2.

The flat subducting geometry described in sector 1 north of 5°N can be related to a portion of over-thickened buoyant oceanic crust, strongly coupled with the overriding plate. Such an interpretation could explain the broad topographic relief of Eastern Cordillera. The anomalous seismicity rate can be referred to massive dehydration process, taking place on the top of the subducting plate.

The differences between sectors 2 and 3 are less evident. A steep Wadati-Benioff zone is present in both sectors, the seismicity rate being lower in sector 3. The Vp pattern changes drastically from a marked low-Vp Wadati-Benioff zone to high-Vp. Given such differences, a second roughly E-W slab tear can be inferred separating sectors 2 and 3 at 3°N (Figure 6.3), even if no correlative tectonic elements can be identified in the seafloor morphology of the downgoing Nazca plate. An alternative hypothesis is that a gradual N-S change in age, thickness and thermal state of the Nazca plate, produces the Vp pattern and the seismicity differences observed between sectors 2 and 3.

## 6.4 Intermediate depth seismicity

As the oceanic lithosphere subducts it undergoes a series of metamorphic phase transformations that release $H_2O$ [Peacock, 1996; Hacker et al., 2003a]. The release of $H_2O$ may enable the generation of intermediate-depth earthquakes by dehydration [Kirby et al., 1996; Hacker et al., 2003b], which in turn may be important for the transport of fluid into the overlying mantle wedge [Davies, 1999]. There is growing evidence that intermediate-depth earthquakes of Wadati-Benioff zones are enabled by dehydration [Green and Houston, 1995; Kirby et al., 1996; Hacker et al., 2003b;

Husen et al., 2003]. In Colombia, the seismicity of the Wadati-Benioff zone shows three different arrangements (Figures 6.3 and 6.4): in the sector 1, where most of the earthquakes occurs (see Chapter 4), the low-angle dipping seismicity relies mostly on a low-velocity zone underlain by high-Vp; in the sector 2 the much steeper seismicity is less concentrated and lies within a low-velocity anomaly to a the depth of 120-130 km; in the sector 3 the seismicity of the Wadati-Benioff zone (dipping as in the sector 2) is poor and relies almost completely on a moderately high-Vp anomaly. The maximum depth of seismicity (180-200 km) is constant for all the sectors.

As described above, intermediate-depth seismicity within the subducting plate may be enabled by dehydration; once the oceanic crust has transformed to anhydrous eclogite dehydration-induced seismicity should stop [Peacock, 1990; Hacker et al., 2003b]. Phase relations predict that oceanic crust transforms to eclogite at shallower depths in warm subduction zones than in cold subduction zones [Peacock and Wang, 1999]. The seismicity volume of sector 1 represents most of the RNSC catalog and concentrates mostly on 100-170 km depth interval. Here it is possible to hypothesize a dramatic and massive dehydration resulting from a delay in eclogitization of the thickened buoyant oceanic crust in a flat-subduction geometry [Pennington, 1984; Sacks, 1983]. The dehydration process is confirmed by a strong high Vp/Vs value just above the bulk of the seismicity, at 70-130 km depth interval (Figure 5.9 and 5.10).

The seismicity of sector 2 and 3 shows, conversely, a continuous and more homogeneous Wadati-Benioff zone. Here a subducting oceanic crust is inferred to be as "normal-thickened", allowing for a gradual and continuous dehydration reactions to

take place with depth, and enabling the fluid migration in the mantle wedge. The Vp/Vs ratio in the sector 2 shows a marked positive anomalies from the slab towards the surface, just below the volcanoes (Figure 5.10), tracing out the fluid pattern.

### 6.4.1 Bucaramanga Nest

The relocated seismicity and the tomographic models show that most of the earthquakes generated in BN volume lies in a strong low-Vp anomaly. The Vp/Vs ratio just above the BN shows a high value, thus indicating a possible presence of fluid released by dehydration reactions within the nest. The cause of such a localized and clustered seismicity is still unclear. Zarifi et al. [2007] suggested that the nest is due to the collision of the Caribbean and the "southern" (i.e. the intra-continental) slab, but clear seismic evidence for the Caribbean Wadati-Benioff plane is lacking, both in their and this data set. A possible explanation for the presence of the BN is the presence of a local compositional and/or rheological heterogeneity in the subducting plate. The seismicity clustered in such a small volume allows to interpret the nest as the result of massive and very localized dehydration phenomenon caused by an anomalous portion of hyper-hydrous subducting oceanic crust, like a volcanic ridge. An alternative and more geologically sounded hypothesis is that the Bucaramanga nest grossly corresponds to the junction with the Merida Andes (see Chapter 2), accommodating the NE-ward displacement of the Maracaibo Block according to both GPS [Trenkamp et al., 2002] and seismic data [Monod et al., 2010]. Therefore the seismic nest could occurs at the contact between the two domains undergoing different geodynamic evolution.

## 6.5 Volcanism

The current understanding of arc magmatism is that fluids released by slab dehydration migrate into the overlying mantle wedge, lower the solidus of the peridotite and trigger partial melting [Gill, 1981]. It is still debated how a partial melt finally ascends through the mantle wedge and reaches the surface. Aqueous fluids and silicate liquids significantly alter the elastic and anelastic properties of rocks, changing the seismic velocities. In recent tomographic studies, low P- and S-wave velocities have been interpreted as indicating the existence of partial melts in the mantle wedge and overlying crust beneath active volcanoes [Iwamori and Zhao, 2000; Nakajima et al., 2001].

In Colombia the best known volcanoes are those located in the segment between 2°N and 5°N, the most studied being the famous Nevado del Ruiz, located in the Central Cordillera. All these volcanic centers are located south of the seismicity offset and overlie steep dipping part of the Nazca slab. The Quaternary rocks are typical subduction calc-alkaline magmatic rocks whose chemistry is interpreted as reflecting fusion of metasomatized mantle wedge followed by fractional crystallization and some assimilation in the crust. The southern volcanic centers in Colombia occur in the Central Cordillera at variable distances above the seismic zone. From north to south, they include Nevado del Huila (2°55' N), the west to east chain known as the Cadena de Los Coconucos (190 km above the seismic zone), and Sotara (2°2'N) (e.g. Marìn-Ceròn [2007]). The more southerly volcanoes (e.g. Dona Juana, Galeras) exhibit features consistent with a transition to a shallower subduction zone [Calvache V and Williams, 1997; Parks et al., 2011] approaching the subduction of flat Carnegie Ridge.

From the tomographic images and relocated seismicity a vertical distance of 170-180 km from the Wadati-Benioff zone (Figure 6.4) for northern and southern volcanic center can be inferred. It was impossible to have indication for the more southerly centers, given the low resolution of tomographic model and the poor station coverage. Tomographic cross sections clearly show a low velocity anomalies beneath volcanoes (sections B-B' and C-C'), at crustal depth and within the uppermost mantle. The Vp/Vs ratio, for the northern volcanoes, shows high values from the Wadati-Benioff plane to the surface, indicating a fluid migration from the slab to the mantle wedge. The absence of volcanism north of 5°N has been related to underplating of the Paleo-Caribbean plate, which may have shielded the rise of magmas [Taboada et al., 2000]. Here, looking at the seismicity distribution and tomographic model, it seems more plausible to relate the change in volcanic style to a marked variation in Mazca subduction dynamics, given the strong complexity and heterogeneity of the downgoing plate. In this view the flat subduction geometry north of 5°N, described above, may have inhibited the formation of volcanic areas. The Vp/Vs ratio pattern observed in Figures 5.9 and 5.10 at 0-50 km depths shows no marked high anomalies north of 5°N, thus indicating a barrier for the fluid migration to shallow depths, maybe due to strong subducting-overriding plate coupling. Such situation avoids the classical mantle wedge hydration and melting and prevents, at present, the development of a volcanic arc.

## 6.6 Comparison with other seismological studies in the Andean margin

Several seismological studies has been performed along the entire Andean margin with both local and teleseismic data. Local tomography and earthquake relocation confirm, in general, the tectonic segmentation described above. Northward from Colombia one of the best studied region, in a seismological sense, is Costa Rica. Here Arroyo et al. [2009], Dinc et al. [2010] and Husen et al. [2003] among others found evidence of a E-NE Cocos dipping slab, which tends to shallow from north to south approaching the subduction of the Cocos ridge. Most of the intermediate-depth seismicity rely on a low-Vp zone and a dehydration mechanism with associated fluid migration were inferred. South of Colombia, seismological studies are lacking for both insufficient seismic network coverage and absence of seismcity (e.g. Perù). More southerly, the subduction in Chile was investigated by Husen et al. [2000] in a combined study onshore and offshore. The tomographic images show a flatly high-Vp body resulting from the subduction of a cold and dense Nazca plate. Few tomography studies in Colombia were performed. Vargas et al. [2007] developed a Vp tomographic model for the southern Colombian Andes, resolving low-Vp anomaly beneath the volcanic areas, in agreement with the results of this study. However, the remaining structural features found by the author do not match with those of this work. This is not surprising, given the better resolving power of the tomographic images of this study, due to the better quality of the actual RSCN dataset. Ojeda and Ottemöller [2002] found high attenuation in the region of present volcanism and in the Western

Cordillera, while in the Eastern Cordillera hte attenuation pattern resulted complex. The existence of a low-angle Caribbean slab beneath NW South America relies upon teleseismic tomography study VanderHilst and Mann [1994], although a seismic Wadati-Benioff zone associated to the postulated slab has remained elusive so far.Gutscher et al. [2000b] related the low angle flat subduction underneath Colombia to the subduction of Caribbean/Choco thickened oceanic crust.

The seismological studies briefly described above (although incompletely) show that tomographic results of this study are in general accordance with the features found in Costa Rica, a region geographically close to Colombia and comparable in the subduction dynamics. Infact, in both regions the subduction results strongly influenced by the structural complexity of the downgoing plate (Cocos for Costa Rica and Nazca for Colombia).

# Chapter 7

# Conclusions

The tomographic models and the relocated seismicity presented in this study show a complex lithospheric structure beneath the Colombian Andes. The complexity results from a strongly heterogeneous subducting Nazca plate. The presence of E-W rift, volcanic ridge and strike-slip faults produces a latitudinal variation in age, thickness and thermal state of the oceanic Nazca plate in the Panama Basin [Lonsdale and Klitgord, 1978]. Such a variation affect the dynamics of subduction producing a segmented belt. The offset in the seismicity and the change in Vp pattern at 5°N clearly separate two distinct tectonic sectors.

North of 5°N (sector 1) the flat subduction of an over-thickened buoyant oceanic lithosphere produces the Eastern Cordillera tectonic assembly with abundant and clustered intermediate-depth seismicity and absence of volcanism. The BN is located inside this sector, in the Cordillera elbow, within a marked low-Vp anomaly.

South of 5°N (sector 2) a 45°east-dipping Wadati-Benioff plane is observed, overlain by a volcanic arc. The seismicity lies within a low-Vp anomaly, plausibly due

to the relatively warm thermal state of subducting oceanic crust. The Vp/Vs ratio shows the fluid migration from the slab towards the mantle wedge, beneath the volcanic chain. The marked differences in seismicity rate, volcanism and Vp pattern between sector 1 and 2 allow to invoke the presence of a slab tear at 5°N oriented roughly E-W. Such a tear is collinear with the Coiba Transorm Fault, a sinistral transform fault which separates the northernmost portion of Nazca plate, namely the Coiba microplate [Sallares and Charvis, 2003].

South of 3°N (sector 3), the seismicity rate is lower and the earthquakes trace out an east-dipping Wadati-Benioff zone relying on a high-Vp amomaly overlain by a volcanic area. Given the differences between sector 2 and 3, a second slab tear, oriented roughly East-West can be inferred. Alternatively, the differences in Vp pattern and seismicity can be produced by a gradual change in lithospheric thickness and thermal state around 3°N.

The seismicity volume of sector 1 represents most of the RNSC catalog and concentrates mostly on 100-170 km depth interval. Here is possible to hypothesize a dramatic and massive dehydration resulting from a delay in eclogitization of the thickened oceanic crust in a flat-subduction geometry [Pennington, 1984; Sacks, 1983]. The seismicity of sector 2 and 3 shows, conversely, a continuous and more homogeneous Wadati-Benioff zone. Here, a "normal-thickened" oceanic crust is still subducting, and allows for a gradual and continuous metamorphic reactions to take place with depth. The BN, located in sector 1, was interpreted as due to the presence of a local heterogeneity in the subducting plate. The seismicity clustered in such a small low-Vp volume, overlain by a a high Vp/Vs ratio, allow to interpret the nest as the

result of massive and very localized dehydration phenomenon caused by an anomalous portion of hyper-hydrous oceanic crust, like a volcanic ridge. An alternative hypothesis is that the Bucaramanga nest grossly corresponds to the junction with the Merida Andes (see Chapter 2), accommodating the NE-ward displacement of the Maracaibo Block according to both GPS [Trenkamp et al., 2002] and seismic data [Monod et al., 2010]. Therefore, the seismic nest could occur at the contact between the two domains undergoing different geodynamic evolution.

The flat subduction geometry north of 5°N may have inhibited the formation of volcanic areas. Vp/Vs ratio pattern observed at 0-50 km depths shows no marked high anomalies north of 5°N, thus indicating a barrier for the fluid migration to shallow depths, maybe due to strong subducting-overriding plate coupling. Such situation avoids the classical mantle wedge hydration and melting and prevents, at present, the development of a volcanic arc.

# Bibliography


Aki, K., Christoffersson, A., Husebye, E., Allmendinger, R., Jordan, T., Kay, S., and Isacks, B. Aki, k. and lee, w., determination of the three-dimensional velocity anomalies under a seis-mic array using first p arrival times from local earthquakes, 1, a homogeneous initial model, journal of geophysical research, 81, 4381–4399, 1976. *Journal of Geophysical Research*, 81:4381–4399, 1976.

Arroyo, I., Husen, S., Flueh, E., Gossler, J., Kissling, E., and Alvarado, G. Three-dimensional p-wave velocity structure on the shallow part of the central costa rican pacific margin from local earthquake tomography using off-and onshore networks. *Geophysical Journal International*, 179(2):827–849, 2009.

Bayona, G., Cortés, M., Jaramillo, C., Ojeda, G., Aristizabal, J., and Reyes-Harker, A. An integrated analysis of an orogen–sedimentary basin pair: Latest cretaceous–cenozoic evolution of the linked eastern cordillera orogen and the llanos foreland basin of colombia. *Geological Society of America Bulletin*, 120(9-10):1171, 2008.

Blot, C. Deep root of andesitic volcanoes: new evidence of magma generation at depth in the benioff zone. *Journal of Volcanology and Geothermal Research*, 10(4): 339–364, 1981a.

Blot, C. Earthquakes at depth beneath volcanoes, forerunners of their activities. application to white island, new zealand. *Journal of Volcanology and Geothermal Research*, 9(4):277–291, 1981b.

Calvache V, M. and Williams, S. Geochemistry and petrology of the galeras volcanic complex, colombia. *Journal of volcanology and geothermal research*, 77(1-4):21–38, 1997.

Carr, M. Nests of intermediate depth (70-160 km) earthquakes adjacent to active volcanoes during 1963-1982. *Journal of volcanology and geothermal research*, 19 (3-4):349–365, 1983.

Colletta, B., Hebrard, F., Letouzey, J., Werner, P., and Rudkiewicz, J. Tectonic style and crustal structure of the eastern cordillera (colombia) from a balanced cross-

section. *Petroleum and tectonics in mobile belts: Paris, Editions Technip*, pages 81–100, 1990.

Cooper, M., Addison, F., Alvarez, R., Coral, M., Graham, R., Hayward, A., Howe, S., Martinez, J., Naar, J., Peñas, R., et al. Basin development and tectonic history of the llanos basin, eastern cordillera, and middle magdalena valley, colombia. *AAPG Bulletin-American Association of Petroleum Geologists*, 79(10):1421–1443, 1995.

Corredor, F. Eastward extent of the late eocene-early oligocene onset of deformation across the northern andes: constraints from the northern portion of the eastern cordillera fold belt, colombia. *Journal of South American Earth Sciences*, 16(6): 445–457, 2003.

Cortés, M., Angelier, J., and Colletta, B. Paleostress evolution of the northern andes (eastern cordillera of colombia): Implications on plate kinematics of the south caribbean region. *Tectonics*, 24(1), 2005.

Crosson, R. Crustal structure modeling of earthquake data 1. simultaneous least squares estimation of hypocenter and velocity parameters. *Journal of geophysical research*, 81(17):3036–3046, 1976.

Davies, J. The role of hydraulic fractures and intermediate-depth earthquakes in generating subduction-zone magmatism. *Nature*, 398(6723):142–145, 1999.

De Boer, J., Defant, M., Stewart, R., Restrepo, J., Clark, L., and Ramirez, A. Quaternary calc-alkaline volcanism in western panama: Regional variation and implication for the plate tectonic framework. *Journal of South American earth sciences*, 1(3): 275–293, 1988.

DeMets, C., Gordon, R., Argus, D., and Stein, S. Current plate motions. *Geophysical journal international*, 101(2):425–478, 1990.

Dengo, C. and Covey, M. Structure of the eastern cordillera of colombia: implications for trap styles and regional tectonics. *AAPG BULLETIN*, 77:1315–1315, 1993.

Dinc, A., Koulakov, I., Thorwart, M., Rabbel, W., Flueh, E., Arroyo, I., Taylor, W., and Alvarado, G. Local earthquake tomography of central costa rica: transition from seamount to ridge subduction. *Geophysical Journal International*, 183(1): 286–302, 2010.

Eberhart-Phillips, D. Three-dimensional velocity structure in northern california coast ranges from inversion of local earthquake arrival times. *Bulletin of the Seismological Society of America*, 76(4):1025–1052, 1986.

Eberhart-Phillips, D. Three-dimensional p and s velocity structure in the coalinga region, california. *Journal of Geophysical Research*, 95(B10):15343–15, 1990.

Engdahl, E. and Scholz, C. A double benioff zone beneath the central aleutians: An unbending of the lithosphere. *Geophysical Research Letters*, 4(10):473–476, 1977.

Evans, J., Eberhart-Phillips, D., Thurber, C., and (US), G. S. *User's manual for SIMULPS12 for imaging Vp and Vp/Vs: a derivative of the" Thurber" tomographic inversion SIMUL3 for local earthquakes and explosions*. US Dept. of the Interior, US Geological Survey, 1994.

Frohlich, C., Kadinsky-Cade, K., and Davis, S. A reexamination of the bucaramanga, colombia, earthquake nest. *Bulletin of the Seismological Society of America*, 85(6): 1622–1634, 1995.

Gailler, A., Charvis, P., and Flueh, E. R. Segmentation of the nazca and south american plates along the ecuador subduction zone from wide angle seismic profiles. *Earth and Planetary Science Letters*, 260(3-4):444–464, 2007. URL `http://linkinghub.elsevier.com/retrieve/pii/S0012821X07003603`.

Gephart, J. Topography and subduction geometry in the central andes: Clues to the mechanics of a noncollisional orogen. *Journal of Geophysical Research*, 99(B6): 12279–12, 1994.

Gill, J. *Orogenic andesites and plate tectonics*, volume 390. Springer-Verlag Berlin, 1981.

Graeber, F. and Asch, G. Three-dimensional models of p wave velocity and p-to-s velocity ratio in the southern central andes by simultaneous inversion of local earthquake data. *Journal of Geophysical Research*, 104(B9):20237–20, 1999.

Green, H. and Houston, H. The mechanics of deep earthquakes. *Annual Review of Earth and Planetary Sciences*, 23:169–214, 1995.

Gusev, A., Radulian, M., Rizescu, M., and Panza, G. Source scaling of intermediate-depth vrancea earthquakes. *Geophysical Journal International*, 151(3):879–889, 2002.

Gutscher, M., Malavieille, J., Lallemand, S., and Collot, J. Tectonic segmentation of the north andean margin: impact of the carnegie ridge collision. *Earth and Planetary Science Letters*, 168(3-4):255–270, 1999.

Gutscher, M., Maury, R., Eissen, J., and Bourdon, E. Can slab melting be caused by flat subduction? *Geology*, 28(6):535, 2000a.

Gutscher, M., Spakman, W., Bijwaard, H., and Hengdahl, R. Geodynamics of flat subduction: seismicity and tomographic constraints from the andean margin. *Tectonics*, 19(5):814–833, 2000b.

Hacker, B., Abers, G., and Peacock, S. Subduction factory 1. theoretical mineralogy, densities, seismic wave speeds, and h2o contents. *J. geophys. Res*, 108(10.1029), 2003a.

Hacker, B., Peacock, S., Abers, G., and Holloway, S. Subduction factory 2. are intermediate-depth earthquakes in subducting slabs linked to metamorphic dehydration reactions. *J. geophys. Res*, 108(10.1029), 2003b.

Hall, M. and Wood, C. Volcano-tectonic segmentation of the northern andes. *Geology*, 13(3):203, 1985.

Haslinger, F. *Velocity structure, seismicity and seismotectonics of Northwestern Greece between the Gulf of Arta and Zakynthos*. PhD thesis, Swiss Federal Institute of Technology Zürich, 1998.

Haslinger, F. and Kissling, E. Investigating effects of 3-d ray tracing methods in local earthquake tomography. *Physics of the Earth and Planetary Interiors*, 123 (2):103–114, 2001.

Havskov, J. and Ottemoller, L. Seisan: The earthquake analysis software version 8.1 user's manual. *University of Bergen, Bergen*, 2005.

Hey, R. Tectonic evolution of the cocos-nazca spreading center. *Bulletin of the Geological Society of America*, 88(10):1404, 1977.

Hoernle, K., van den Bogaard, P., Werner, R., Lissinna, B., Hauff, F., Alvarado, G., and Garbe-Schönberg, D. Missing history (16–71 ma) of the galápagos hotspot: Implications for the tectonic and biological evolution of the americas. *Geology*, 30 (9):795, 2002.

Husen, S., Kissling, E., and Flueh, E. Local earthquake tomography of shallow subduction in north chile- a combined onshore and offshore study. *Journal of Geophysical Research*, 105(B12):28183–28198, 2000.

Husen, S., Quintero, R., Kissling, E., and Hacker, B. Subduction-zone structure and magmatic processes beneath costa rica constrained by local earthquake tomography and petrological modelling. *Geophysical Journal International*, 155(1):11–32, 2003.

INGEOMINAS. Microzonificacion sismica de santa fe de bogota.crustal structure and local seismicity in colombia. 1997.

Isacks, B. Uplift of the central andean plateau and bending of the bolivian orocline. *Journal of Geophysical Research*, 93(B4):3211–3231, 1988.

Iwamori, H. and Zhao, D. Melting and seismic structure beneath the northeast japan arc. *Geophysical research letters*, 27(3):425–428, 2000.

Jaramillo, J., Linero, P., and Garver, J. Neogene's volcanism in the cordillera oriental of the andes, colombia. *Earth Sciences Research Journal*, 9(1):19, 2005.

Jordan, T., Isacks, B., Allmendinger, R., Brewer, J., RAMOS, V., and Ando, C. Andean tectonics related to geometry of subducted nazca plate. *Geological Society of America Bulletin*, 94(3):341–361, 1983.

Jung, H., Green Ii, H., and Dobrzhinetskaya, L. Intermediate-depth earthquake faulting by dehydration embrittlement with negative volume change. *Nature*, 428(6982): 545–549, 2004.

Kirby, S., Stein, S., Okal, E., and Rubie, D. Metastable mantle phase transformations and deep earthquakes in subducting oceanic lithosphere. *Reviews of geophysics*, 34 (2):261–306, 1996.

Kissling, E. Geotomography with local earthquake data. *Reviews of Geophysics*, 26 (4):659–698, 1988.

Kissling, E., Ellsworth, W., Eberhart-Phillips, D., and Kradolfer, U. Initial reference models in local earthquake tomography. 1994.

Kissling, E., Husen, S., and Haslinger, F. Model parametrization in seismic tomography: a choice of consequence for the solution quality. *Physics of the Earth and Planetary Interiors*, 123(2):89–101, 2001.

Kolarsky, R., Mann, P., and Montero, W. Island arc response to shallow subduction of the cocos ridge, costa rica. *SPECIAL PAPERS-GEOLOGICAL SOCIETY OF AMERICA*, pages 235–235, 1995.

Koulakov, I., Zaharia, B., Enescu, B., Radulian, M., Popa, M., Parolai, S., and Zschau, J. Delamination or slab detachment beneath vrancea? new arguments from local earthquake tomography. *Geochem. Geophy. Geosy*, 11:Q03002, 2010.

Lahr, J. *HYPOELLIPSE: A Computer Program for Determining Local Earthquake Hypocentral Parameters, Magnitude, and First-Motion Pattern, Y2K Compliant Version*. US Dept. of the Interior, US Geological Survey, 1999.

Lee, W., Lahr, J., and for Earthquake Research, N. C. *HYPO71 (revised): a computer program for determining hypocenter, magnitude, and first motion pattern of local earthquakes*. US Dept. of the Interior, Geological Survey, National Center for Earthquake Research, 1975.

Lonsdale, P. Creation of the cocos and nazca plates by fission of the farallon plate. *Tectonophysics*, 404(3-4):237–264, 2005.

Lonsdale, P. and Klitgord, K. Structure and tectonic history of the eastern panama basin. *Geological Society of America Bulletin*, 89(7):981, 1978.

Marìn-Ceròn, M. Major, trace element and multi-isotopic systematics of sw colombian volcanic arc, northern andes, implication for the stability of carbonate-rich sediment at subduction zone and the genesis of andesite magma [ph.d. thesis]. 2007.

McCann, W., Nishenko, S., Sykes, L., and Krause, J. Seismic gaps and plate tectonics: seismic potential for major boundaries. *pure and Applied Geophysics*, 117(6):1082–1147, 1979.

McGeary, S., Nur, A., and Ben-Avraham, Z. Spatial gaps in arc volcanism: The effect of collision or subduction of oceanic plateaus. *Tectonophysics*, 119(1-4):195–221, 1985.

Menke, W. *Geophysical data analysis: discrete inverse theory*, volume 45. Academic Pr, 1989.

Michelini, A. and McEvilly, T. Seismological studies at parkfield. i. simultaneous inversion for velocity structure and hypocenters using cubic b-splines parameterization. *Bulletin of the Seismological Society of America*, 81(2):524–552, 1991.

Monod, B., Dhont, D., and Hervouët, Y. Orogenic float of the venezuelan andes. *Tectonophysics*, 490(1):123–135, 2010.

Mora, A., Parra, M., Strecker, M., Kammer, A., Dimaté, C., and Rodríguez, F. Cenozoic contractional reactivation of mesozoic extensional structures in the eastern cordillera of colombia. *Tectonics*, 25(2):1–19, 2006.

Mora, A., Gaona, T., Kley, J., Montoya, D., Parra, M., Quiroz, L., Reyes, G., and Strecker, M. The role of inherited extensional fault segmentation and linkage in contractional orogenesis: a reconstruction of lower cretaceous inverted rift basins in the eastern cordillera of colombia. *Basin Research*, 21(1):111–137, 2009.

Mora, A., Horton, B., Mesa, A., Rubiano, J., Ketcham, R., Parra, M., Blanco, V., Garcia, D., and Stockli, D. Migration of cenozoic deformation in the eastern cordillera of colombia interpreted from fission track results and structural relationships: Implications for petroleum systems. *AAPG bulletin*, 94(10):1543, 2010.

Müller, R., Royer, J., Cande, S., Roest, W., and Maschenkov, S. New constraints on the late cretaceous/tertiary plate tectonic evolution of the caribbean. *Sedimentary Basins of the World*, 4:33–59, 1999.

Nakajima, J., Matsuzawa, T., Hasegawa, A., and Zhao, D. Seismic imaging of arc magma and fluids under the central part of northeastern japan. *Tectonophysics*, 341(1-4):1–17, 2001.

Nieto, A. and Escallon, J. The new colombian seismological network. *Geophys. Int*, 35:53–57, 1996.

Ojeda, A. and Havskov, J. Crustal structure and local seismicity in colombia. *Journal of seismology*, 5(4):575–593, 2001.

Ojeda, A. and Ottemöller, L. ¡ i¿ q¡/i¿¡ sub¿ lg¡/sub¿ tomography in colombia. *Physics of the Earth and Planetary Interiors*, 130(3):253–270, 2002.

Ojeda, A., Martinez, S., Bermudez, M., and Atakan, K. The new accelerograph network for santa fe de bogota, colombia and implications for microzonation. *Soil Dynamics and Earthquake Engineering*, 22(9-12):791–797, 2002.

Pardo, N., Cepeda, H., and Jaramillo, J. The paipa volcano eastern cordillera of colombia, south america, volcanic stratigraphy. *Earth Sciences Research Journal*, 9(1):3, 2005.

Parks, M., Biggs, J., Mather, T., Pyle, D., Amelung, F., Monsalve, M., and Medina, L. Co-eruptive subsidence at galeras identified during an insar survey of colombian volcanoes (2006-2009). *Journal of Volcanology and Geothermal Research*, 2011.

Parra, M., Mora, A., Jaramillo, C., Strecker, M., Sobel, E., Quiroz, L., Rueda, M., and Torres, V. Orogenic wedge advance in the northern andes: Evidence from the oligocene-miocene sedimentary record of the medina basin, eastern cordillera, colombia. *Bulletin of the Geological Society of America*, 121(5-6):780, 2009.

Pavlis, G. and Booker, J. The mixed discrete-continuous inverse problem: application to the simultaneous determination of earthquake hypocenters and velocity structure. *Journal of Geophysical Research*, 85(B9):4801–4810, 1980.

Peacock, S. Fluid processes in subduction zones. *Science*, 248(4953):329, 1990.

Peacock, S. Thermal and petrologic structure of subduction zones. *Geophysical monograph*, 96:119–133, 1996.

Peacock, S. and Wang, K. Seismic consequences of warm versus cool subduction metamorphism: Examples from southwest and northeast japan. *Science*, 286(5441): 937, 1999.

Pegler, G. and Das, S. An enhanced image of the pamir–hindu kush seismic zone from relocated earthquake hypocentres. *Geophysical Journal International*, 134(2): 573–595, 1998.

Pennington, W. Subduction of the eastern panama basin and seismotectonics of northwestern south america. *Journal of Geophysical Research*, 86(B11):10753–10, 1981.

Pennington, W. The effect of oceanic crustal structure on phase changes and subduction. *Tectonophysics*, 102(1-4):377–398, 1984.

Pennington, W., Mooney, W., van Hissenhoven, R., Meyer, H., Ramirez, J., and Meyer, R. Results of a reconnaissance microearthquake survey of bucaramanga, colombia. *Geophysical Research Letters*, 6(2):65–68, 1979.

Pindell, J. and Barrett, S. Geological evolution of the caribbean region: a plate tectonic perspective. *The Caribbean region: Boulder, Colorado, Geological Society of America, Geology of North America, v. H*, pages 405–432, 1990.

Preston, L., Creager, K., Crosson, R., Brocher, T., and Trehu, A. Intraslab earthquakes: dehydration of the cascadia slab. *Science*, 302(5648):1197, 2003.

Protti, M., Schwartz, S., and Zandt, G. Simultaneous inversion for earthquake location and velocity structure beneath central costa rica. *Bulletin of the Seismological Society of America*, 86(1A):19–31, 1996.

Pulido, N. Seismotectonics of the northern andes (colombia) and the development of seismic networks. *Bulletin of the International Institute of Seismology and Earthquake Engineering, Special Edition, p69-76*, 2003.

Reyners, M. Plate coupling and the hazard of large subduction thrust earthquakes at the hikurangi subduction zone, new zealand. *New Zealand Journal of Geology and Geophysics*, 41(4):343–354, 1998.

Reyners, M., Eberhart-Phillips, D., and Stuart, G. A three-dimensional image of shallow subduction: crustal structure of the raukumara peninsula, new zealand. *Geophysical Journal International*, 137(3):873–890, 1999.

Sacks, I. The subduction of young lithosphere. *Journal of Geophysical Research*, 88 (B4):3355–3366, 1983.

Sallares, V. and Charvis, P. Crustal thickness constraints on the geodynamic evolution of the galapagos volcanic province. *Earth and Planetary Science Letters*, 214(3-4): 545–559, 2003.

Sarmiento, L. *Mesozoic Rifting and Cenozoic Basin Inversion History of the Eastern Cordillera, Colombian Andes-Inferences from tectonic models*. PhD thesis, Tesis Ph. D., Netherlands Research School of Sedimentary Geology, 295p.[Links], 2001.

Schneider, J., Pennington, W., and Meyer, R. Seismicity and tectonics of western venezuela. *Journal of Geophysical Research*, 62:1711–1752, 1972.

Schneider, J., Pennington, W., and Meyer, R. Microseismicity and focal mechanisms of the intermediate-depth bucaramanga nest, colombia. *Journal of Geophysical Research*, 92(B13):13913–13, 1987.

Shearer, P. *Introduction to seismology*. Cambridge Univ Pr, 1999.

Sillitoe, R. Tectonic segmentation of the andes: implications for magmatism and metallogeny. *Nature*, 250:542–545, 1974.

Stoiber, R. and Carr, M. Quaternary volcanic and tectonic segmentation of central america. *Bulletin of Volcanology*, 37(3):304–325, 1973.

Taboada, A., Rivera, L., Fuenzalida, A., Cisternas, A., Philip, H., Bijwaard, H., Olaya, J., and Rivera, C. Geodynamics of the northern andes: Subductions and intracontinental deformation (colombia). *Tectonics*, 19(5):787–813, 2000.

Thurber, C. and Eberhart-Phillips, D. Local earthquake tomography with flexible gridding. *Computers & Geosciences*, 25(7):809–818, 1999.

Thurber, C. Earthquake locations and three-dimensional crustal structure in the coyote lake area, central california. *Journal of Geophysical Research*, 88(B10): 8226–8236, 1983.

Toomey, D. and Foulger, G. Tomographic inversion of local earthquake data from the hengill-grensdalur central volcano complex, iceland. *Journal of Geophysical Research*, 94(B12):17–497, 1989.

Trenkamp, R., Kellogg, J., Freymueller, J., and Mora, H. Wide plate margin deformation, southern central america and northwestern south america, casa gps observations. *Journal of South American Earth Sciences*, 15(2):157–171, 2002.

Tryggvason, E. and Lawson Jr, J. The intermediate earthquake source near bucaramanga, colombia. *Bulletin of the Seismological Society of America*, 60(1):269–276, 1970.

Um, J. and Thurber, C. A fast algorithm for two-point seismic ray tracing. *Bulletin of the Seismological Society of America*, 77(3):972–986, 1987.

Usami, T. and Watanabe, T. Definition and characteristic features of a seismically active region (earthquake nest) in the kanto district. *Pure and Applied Geophysics*, 118(2):1326–1328, 1980.

VanderHilst, R. and Mann, P. Tectonic implications of tomographic images of subducted lithosphere beneath northwestern south america. *Geology*, 22(5):451, 1994.

Vargas, C. Tomographic constraints on subducted slabs beneath colombia: Implications for tectonics and exploration. *XIV Congreso Latinoamericano de Geologia*, (XIV):22, 2011.

Vargas, C., Pujades, L., and Montes, L. Seismic structure of south-central andes of colombia by tomographic inversion. *Geofísica internacional*, 46(2):117–127, 2007.

Virieux, J., Farra, V., et al. Ray tracing in 3-d complex isotropic media: An analysis of the problem. *Geophysics*, 56(12):2057–2069, 1991.

Wortel, M. Spatial and temporal variations in the andean subduction zone. *Journal of the Geological Society*, 141(5):783, 1984.

Zarifi, Z. Unusual subduction zones: Case studies in colombia and iran [ph.d. thesis]. 2007.

Zarifi, Z. and Havskov, J. Characteristics of dense nests of deep and intermediate-depth seismicity. *Advances in geophysics*, 46:237–278, 2003.

Zarifi, Z., Havskov, J., and Hanyga, A. An insight into the bucaramanga nest. *Tectonophysics*, 443(1-2):93–105, 2007.

Zhao, D. Global tomographic images of mantle plumes and subducting slabs: insight into deep earth dynamics. *Physics of the Earth and Planetary Interiors*, 146(1-2): 3–34, 2004.

Zhao, D., Hasegawa, A., and Horiuchi, S. Tomographic imaging of p and s wave velocity structure beneath northeastern japan. *Journal of Geophysical Research*, 97(B13):19909–19, 1992.

Zhao, D., Christensen, D., and Pulpan, H. Tomographic imaging of the alaska subduction zone. *Journal of Geophysical Research*, 100(B4):6487–6504, 1995.

# Appendix A

# RSNC station list

Table A.1: List of RSNC permanent stations.

| Station | Longitude (deg) | Latitude (deg) | Altitude (m) |
|---|---|---|---|
| BAR2 | -73.18 | 6.58 | 1864 |
| BET | -75.44 | 2.68 | 540 |
| BRR | -73.71 | 7.11 | 137 |
| BTL | -73.27 | 6.92 | 1874 |
| CAP2 | -77.36 | 8.65 | 229 |
| CHI | -73.33 | 4.63 | 3140 |
| CRU | -76.95 | 1.57 | 2761 |
| CTAB | -74.20 | 5.01 | 3500 |
| CTAU | -73.19 | 7.08 | 1164 |
| CUM | -77.83 | 0.94 | 3420 |
| DBB | -76.21 | 7.02 | 756 |
| FLO2 | -75.65 | 1.58 | 365 |
| GIR2 | -73.19 | 7.08 | 1164 |
| GOR | -78.17 | 3.00 | 63 |
| GRA | -72.80 | 7.88 | 1275 |
| GUA | -72.63 | 2.54 | 217 |
| GUE | -72.92 | 7.83 | 2430 |
| GUY | -75.37 | 5.23 | 3600 |
| HEL | -75.53 | 6.19 | 2815 |
| MAL | -77.34 | 4.01 | 75 |
| MAP | -81.61 | 4.00 | 137 |
| MON | -75.66 | 8.77 | 500 |
| MUN | -76.96 | 2.47 | 3010 |
| NOR | -74.87 | 5.57 | 536 |
| OCA | -73.32 | 8.24 | 1264 |

Continued on next page

**Table A.1 – continued from previous page**

| Station | Longitude (deg) | Latitude (deg) | Altitude (m) |
|---|---|---|---|
| PAL | -76.28 | 4.90 | 704 |
| PAM | -72.62 | 7.38 | 2291 |
| POP2 | -76.68 | 2.54 | 1869 |
| PRA | -74.89 | 3.71 | 458 |
| PTB | -74.27 | 6.32 | 260 |
| RAG | -72.5 | 7.63 | 1468 |
| ROSC | -74.33 | 4.86 | 3020 |
| RUS | -73.08 | 5.89 | 3697 |
| SAN | -73.07 | 6.76 | 1608 |
| SJC | -75.18 | 9.90 | 597 |
| SOL | -77.41 | 6.23 | 38 |
| TOL | -75.32 | 4.59 | 2577 |
| TUM | -78.73 | 1.84 | 50 |
| URI | -71.99 | 11.70 | 68 |
| YOP | -72.35 | 5.35 | 961 |
| YOT | -76.207 | 3.59 | 1040 |
| ZAR | -74.848 | 7.49 | 185 |

# Appendix B

# TOMO Station list

Table B.1: List of station used in the tomographic inversion, including station out of national boundary, volcanological observatories and temporary network.

| **Station** | **Longitude (deg)** | **Latitude (deg)** | **Altitude (m)** |
|---|---|---|---|
| ROSC | -74.32 | 4.84 | 2987 |
| RUS | -73.083 | 5.8925 | 3697 |
| TOL | -75.32 | 4.58533 | 2577 |
| BAR | -73.182 | 6.59233 | 1877 |
| HEL | -75.529 | 6.19083 | 2815 |
| PRA | -74.886 | 3.714 | 457 |
| OCA | -73.319 | 8.23883 | 1264 |
| GUA | -72.627 | 2.54483 | 217 |
| CHI | -73.732 | 4.6295 | 3140 |
| FLO | -75.653 | 1.5825 | 360 |
| MORA | -75.368 | 4.46317 | 2280 |
| MAL | -77.335 | 4.013 | 75 |
| POP | -76.525 | 2.44383 | 2045 |
| CUM | -77.825 | 0.940833 | 3420 |
| SANL | -75.399 | 4.46033 | 2200 |
| LAJA | -75.416 | 4.49583 | 2600 |
| NIDO | -75.327 | 4.664 | 4715 |
| ESME | -75.352 | 4.6645 | 4490 |
| ALF2 | -75.34 | 4.86883 | 4760 |
| BIS | -75.339 | 4.89433 | 5030 |
| OLLE | -75.359 | 4.902 | 4630 |
| LISA | -75.334 | 4.91533 | 4700 |
| TOLD | -75.399 | 4.943 | 3760 |

Continued on next page

**Table B.1 – continued from previous page**

| Station | Longitude (deg) | Latitude (deg) | Altitude (m) |
|---|---|---|---|
| CERR | -75.288 | 5.08083 | 3768 |
| SOL | -77.409 | 6.2265 | 38 |
| CRU | -76.951 | 1.56767 | 2761 |
| GCAL | -77.423 | 1.21383 | 2353 |
| ANIL | -75.402 | 4.491 | 2300 |
| SANJ | -75.376 | 4.52217 | 2400 |
| OLLB | -75.359 | 4.902 | 4630 |
| KEN | -74.048 | 11.1108 | 2560 |
| 1151 | -73.731 | 4.633 | 3100 |
| CIMA | -75.393 | 4.491 | 2700 |
| TUM | -78.726 | 1.8355 | 50 |
| MON | -75.658 | 8.77383 | 500 |
| CAP2 | -77.36 | 8.64567 | 229 |
| RREF | -75.347 | 4.90083 | 4743 |
| BRR | -73.712 | 7.1075 | 137 |
| VR2Z | -76.035 | 2.97233 | 4544 |
| PCON | -76.397 | 2.32767 | 4294 |
| BET | -75.441 | 2.68133 | 540 |
| UPD1 | -78.014 | 8.54867 | 74 |
| BCIP | -79.84 | 9.17 | 61 |
| PINA | -80.064 | 9.254 | 0 |
| SOTA | -76.608 | 2.135 | 3795 |
| GCUF | -77.345 | 1.226 | 3800 |
| FLO2 | -75.653 | 1.58267 | 365 |
| POP2 | -76.676 | 2.54017 | 1869 |
| DBB | -76.21 | 7.0175 | 756 |
| URI | -71.993 | 11.7017 | 68 |
| YOP | -72.421 | 5.35317 | 933 |
| RAG | -72.499 | 7.62967 | 1468 |
| GUE | -72.925 | 7.83017 | 2430 |
| GRA | -72.804 | 7.88467 | 1275 |
| BRI | -72.797 | 7.7165 | 1427 |
| VR2E | -76.035 | 2.97233 | 4544 |
| NOR | -74.873 | 5.566 | 536 |
| SDV | -70.63 | 8.88 | 1620 |
| OTAV | -78.451 | 0.237667 | 3492 |
| CLIM | -77.887 | 0.941333 | 4232 |
| GUY | -75.368 | 5.2265 | 3600 |
| BTL | -73.268 | 6.9185 | 1874 |

Continued on next page

**Table B.1 – continued from previous page**

| **Station** | **Longitude (deg)** | **Latitude (deg)** | **Altitude (m)** |
|---|---|---|---|
| GIR | -73.197 | 7.08033 | 1396 |
| BAR2 | -73.184 | 6.59167 | 1864 |
| GIR2 | -73.193 | 7.07883 | 1164 |